AD-A206 991

(2)

REPORT DOCUMENTATION PAGE

DTIC ELECTE APR 18 1989 S D

1a. REPORT SECURITY CLASSIFICATION: Unclassified	1b RESTRICTIVE MARKINGS: None
2a. SECURITY CLASSIFICATION AUTHORITY: Unclassified	3 DISTRIBUTION/AVAILABILITY OF REPORT: Approved for public release, Unlimited distribution unlimited
2b. DECLASSIFICATION/DOWNGRADING SCHEDULE	
4. PERFORMING ORGANIZATION REPORT NUMBER(S)	5 MONITORING ORGANIZATION REPORT NUMBER(S): AFOSR-TR. 89-0462
6a. NAME OF PERFORMING ORGANIZATION: A.H. Nayfeh, Dept. of Aero/Eng. Mech	6b. OFFICE SYMBOL (If applicable):
7a NAME OF MONITORING ORGANIZATION: AFOSR/NE	
6c. ADDRESS (City, State, and ZIP Code): Mail Location 70, University of Cincinnnati, Cincinnati, Ohio 45221	7b ADDRESS (City, State, and ZIP Code): Building 410, Bolling Air Force Base, DC 20332-6448
8a. NAME OF FUNDING/SPONSORING ORGANIZATION: AFOSR	8b OFFICE SYMBOL (If applicable): NE
9 PROCUREMENT INSTRUMENT IDENTIFICATION NUMBER: AFOSR-86-0052	
8c. ADDRESS (City, State, and ZIP Code): Building 410, Bolling Air Force Base, DC 20332-6448	10. SOURCE OF FUNDING NUMBERS: PROGRAM ELEMENT NO 61102F; PROJECT NO. 2306; TASK NO. A3; WORK UNIT ACCESSION NO.

11 TITLE (Include Security Classification)

Interactions of Ultrasonic Waves with Composite Plates

12 PERSONAL AUTHOR(S)

A.H. Nayfeh

13a TYPE OF REPORT	13b TIME COVERED	14 DATE OF REPORT (Year, Month, Day)	15. PAGE COUNT
Final Scientific	FROM 12/85 TO 12/88	24 March 89	64

16. SUPPLEMENTARY NOTATION

17. COSATI CODES			18 SUBJECT TERMS (Continue on reverse if necessary and identify by block number)
FIELD	GROUP	SUB-GROUP	Waves, Ultrasonic, Composites, Leaky

19. ABSTRACT (Continue on reverse if necessary and identify by block number)

We present a unified analytical treatment of the interaction of ultrasonic waves with single and multilayered arbitrarily oriented anisotropic elastic plates. The individual components forming the plate are allowed to possess up to as low as monoclinic symmetry. The plates are assumed to be immersed in a fluid and subjected to incident acoustic waves at arbitrary angles from the normal as well as at arbitrary aximuthal angles. Reflection and transmission coefficients are derived from which all propagation characteristics are identified. Highly complex reflection behavior, expressed as phase velocity-frequency dispersion, is observed as a consequence of anisotropy. Extensive comparisons with the concurrently acquired experimental data by Chimenti at the AFWAL on a variety of composite samples have been of unique help in assessing the validity of our theoretical modeling, and its potential application in the nondestructive evaluation of materials.

20 DISTRIBUTION/AVAILABILITY OF ABSTRACT	21 ABSTRACT SECURITY CLASSIFICATION
☒ UNCLASSIFIED/UNLIMITED ☐ SAME AS RPT. ☐ DTIC USERS	Unclassified
22a NAME OF RESPONSIBLE INDIVIDUAL: A.H. Nayfeh WEINSTOCK	22b TELEPHONE (Include Area Code): (513)556-3557 202-767-4933 / 22c OFFICE SYMBOL: NE

DD FORM 1473, 84 MAR 83 APR edition may be used until exhausted. All other editions are obsolete.

SECURITY CLASSIFICATION OF THIS PAGE

UNCLASSIFIED

89 4 9

"INTERACTIONS OF ULTRASONIC WAVES WITH COMPOSITE PLATES"

A final report

Submitted to the Air Force Office of Scientific Research

Grant NO. AFOSR-86-0052

December 1985 - December 1988

by

Adnan H. Nayfeh

Department of Aerospace Engineering

and Engineering Mechanics

University of Cincinnati

Cincinnati, OH 45221

March 1989

ABSTRACT

We present a unified analytical treatment of the interaction of ultrasonic waves with single and multilayered arbitrarily oriented anisotropic elastic plates. The individual components forming the plate are allowed to posses up to as low as monoclinic symmetry. The plates are assumed to be immersed in a fluid and subjected to incident acoustic waves at arbitrary angles from the normal as well as at arbitrary azimuthal angles. Reflection and transmission coefficients are derived from which all propagation characteristics are identified. Highly complex reflection behavior, expressed as phase velocity-frequency dispersion, is observed as a consequence of anisotropy. Extensive comparisons with the concurrently acquired experimental data by Chimenti at the AFWAL on a variety of composite samples have been of unique help in assessing the validity of our theoretical modeling, and its potential application in the nondestructive evaluation of materials.

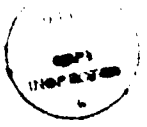

I. INTRODUCTION

In recent years considerable efforts have been expended upon the modeling, testing and analysis of fibrous composites. This is due in part to their popularity in applications requiring high stiffness to weight ratios and also to their intrinsic interest as challenging mechanical systems. However, the morphology of fiber-reinforced composites, as compared with that of homogeneous isotropic media, can seriously complicate their mechanical response. For example, these materials differ from isotropic homogeneous materials in that they are anisotropic and dispersive. The degrees of anisotropy and dispersivity depend upon the specific material under consideration and also upon the specific application, however.

Since most fibrous structural components are subjected to cyclic or impulsive loads which can lead to degradation in load-carrying capability, initial inspection and continued monitoring of these materials for detection and sizing of strength-degrading flaws is necessary in order to insure structural reliability. Ultrasonic nondestructive evaluation is one useful means to provide information related to structural integrity of composites. To assist in the exploitation of this technique for inspecting composites, a full understanding of the propagation of elastic waves in fibrous composites is highly desirable.

Compared with the voluminous literature on the propagation of elastic waves in isotropic media, a limited amount of work exists on anisotropic materials. This is particularly true for the classes of guided waves such as surface, Love, Lamb, and Stonely waves. Investigation of the propagation of bulk waves in anisotropic materials is relatively well established (see, for example, Musgrave [1], Synge [2] and Fedorov [3]). Comparatively

speaking, few quantitative results have been reported on solutions of guided waves in anisotropic media.

Several authors [4-14] have discussed the reflection and refraction problems from interfaces of anisotropic media in varying degrees of detail. Stonely, in 1955, studied Rayleigh surface wave propagation on an anisotropic half-space having cubic crystal symmetry [15]. Since then several other authors [16-22] have considered and reported on similar problems. Theoretical analyses have been undertaken for free Lamb waves in plates of orthotropic [23-24] , transversely isotropic [25-27] and cubic [28-29] materials. Some limited approximate theoretical and experimental results for wave propagation in thin (small values of fd where f is the frequency and d is the plate thickness) orthotropic plates with arbitrary orientations have been presented [30-32].

Because fiber-reinforced composites are often employed in plate-like structures and ultrasonic testing is conveniently performed in immersion, we recently investigated both theoretically and experimentally the behavior of guided elastic waves in liquid-coupled plates of unidirectional fibrous composites [33,34]. For consistency we refer, in our work, to the liquid-coupled modes as plate modes. Hereafter, we refer to liquid or fluid coupling synonomously. These excitations may be contrasted with Lamb modes for a plate in vacuum, like that studied in [35,36]. In [33,34] results were presented for cases where the plate wave vector is along the direction of symmetry, i.e., the fiber axis.

As compared with isotropic cases, solutions to the anisotropic problem are much more difficult to obtain. This is because of the added algebraic complications in handling of the pertinent equations. Based on the widely used slowness wave surface techniques [1-3] several differences between the

wave propagation characteristics of isotropic and anisotropic media can be identified. In the isotropic case, the slowness surface consists of two concentric spherical sheets, the inner one represents longitudinal wave and the outer represents two coincident shear waves. For the anisotropic case however, there are three general surfaces, one for a quasi longitudinal and two for quasi shear waves. This means that incident and reflected waves in anisotropic media can no longer be thought of as purely longitudinal or shear with appropriate directionally independent wave speeds. This also implies that the direction of energy flow (i.e., group velocity) does not, in general, coincide with the normal to the wave front [3]. The uncoupling of the longitudinal and shear potentials in the isotropic case simplifies the algebraic treatment of their wave propagation characteristics compared to the corresponding anisotropic case. Generally speaking, in the case of anisotropic media equations describing the motions of the three waves are coupled, and in order to identify them one needs to solve a sixth order polynomial characteristic equation. For special material symmetry directions the equation of one of the shear waves uncouple, leading to fourth order polynomial equations which are relatively easier to handle. Taken together these complications perhaps explain why many of the available treatments of wave propagation in anisotropic media emphasize wave motions along material symmetry directions.

In this report we develop complete analysis for the propagation of guided waves in a liquid-coupled, arbitrarily oriented single and multilayered anisotropic plates. The wave is allowed to be incident at an arbitrary direction on the plate (i.e., for arbitrary incident and azimuthal angle). The solutions obtained will thus include, as special cases, those pertaining to higher symmetry materials such as ortotropic, transversely

isotropic (an example of which is unidirectionally reinforced composite), cubic, and isotropic media. The reflection and the transmission coefficients are derived, and algebraic expressions for the characteristic symmetric and antisymmetric plate modes are found possible for the single layer plate system. Detailed comparisons are presented between the experimental data of Chimenti and the theory on a variety of composite sapmles as representatives of anisotropic media are presented.

Typically a layered medium consists of two or more material components attached at their interfaces in some fashion. Generally speaking, for wave propagation in such media our solutions are obtained by expressing the displacements and stresses in each component in terms of its wave amplitudes. By satisfying appropriate interfacial conditions, characteristic equations are constructed which involve the amplitudes of all layers. This constitutes the direct approach. The degree of complication in the algebraic manipulation of the analysis will thus depend upon the number of components. For relatively few components, the direct approach is appropriate. However, as the number of components increases the direct approach becomes cumbersome, and one may resort to the alternative matrix transfer technique introduced originally by Thomson [37]. According to this technique one constructs the propagation matrix for a stack of an arbitrary number of layers by extending the solution from one layer to the next while satisfying the appropriate interfacial continuity conditions. In this report we use both the direct and matrix transfer methods in order to obtain solutions for the single layer plate and the multilayered ones, respectively.

A key condition which is found to facilitate our analysis is the fact that the wave vectors of the incident and refracted waves must all lie in

the same plane. This result is a consequence of satisfying continuity conditions at the liquid-solid interface (see [10] for justification). We will therefore conduct our analysis in a coordinate system formed by incident and interfacial planes rather than by material symmetry axes. This expedient leads to a simplification in our algebraic analysis and computations.

II. THEORETICAL ANALYSIS

1. THE SINGLE PLATE CASE

In this section we present theoretical and experimental studies of the interaction of ultrasonic waves with generally oriented monoclinic elastic plates immersed in liquid. The analysis yields exact calculation of the reflected and transmitted partial waves. The plane of incidence of the acoustic wave makes an arbitrary angle with respect to material symmetry axis, resulting in coupling of the equations describing the motion of the vertically and horizontally polarized waves in the plates. Highly complex reflection behavior, expressed in velocity dispersion, is observed in the model prediction. Comparisons are made to extensive experimental data collected by Chimenti in ultrasonic reflection measurements on a plate of T300/Ciba-Geigy 914 composite, selected as a model system to test the theory. Excellent agreement is seen in curves at several azimuthal angles between 0° and 90°, despite the complicated behavior of the propagation.

1.1 Formulation of the problem

Consider an infinite anisotropic plate having the thickness d and immersed in fluid such that its symmetry axes are oriented originally along the cartesian coordinate system $x_i' = (x_1', x_2', x_3')$. The plane x_1'-x_2' is chosen

to coincide with the upper surface of the plate, and the x_3' coordinate is normal to it, as illustrated in Fig. 1.1. With respect to this primed coordinate system, the elastic field equations of the plate are given by the momentum equations

$$\frac{\partial \sigma_{ij}'}{\partial x_j'} = \rho' \frac{\partial^2 u_i'}{\partial t^2} \qquad (1.1)$$

and, from the general constitutive relations for anisotropic media,

$$\sigma_{ij}' = c_{ijk\ell}' \, e_{k\ell}' \qquad (1.2)$$

by the specialized expanded matrix form to orthotropic media

$$\begin{vmatrix} \sigma_{11}' \\ \sigma_{22}' \\ \sigma_{33}' \\ \sigma_{23}' \\ \sigma_{13}' \\ \sigma_{12}' \end{vmatrix} = \begin{vmatrix} C_{11}' & C_{12}' & C_{13}' & 0 & 0 & C_{16}' \\ C_{12}' & C_{22}' & C_{23}' & 0 & 0 & C_{26}' \\ C_{13}' & C_{23}' & C_{33}' & 0 & 0 & C_{36}' \\ 0 & 0 & 0 & C_{44}' & C45' & 0 \\ 0 & 0 & 0 & C_{45}' & C_{55}' & 0 \\ C_{16}' & C_{26}' & C_{36}' & 0 & 0 & C_{66}' \end{vmatrix} \begin{vmatrix} e_{11}' \\ e_{22}' \\ e_{33}' \\ \gamma_{23}' \\ \gamma_{13}' \\ \gamma_{12}' \end{vmatrix} \qquad (1.3)$$

where we used the contracting subscript notations 1→11, 2→22, 3→33, 4→23, 5→13 and 6→12 to relate $c_{ijk\ell}'$ to C_{pq}' (i,j,k,ℓ = 1,2,3 and p,q = 1,2....6). Thus, C_{55}' stands for c_{1313}', for example. Here σ_{ij}', e_{ij}' and u_i' are the components of stress, strain and displacement, respectively, and ρ' is the material density. In Eq. (1.3), $\gamma_{ij}' = 2e_{ij}'$ (with i≠j) defines the engineering shear strain components.

Since $c'_{ijk\ell}$ is a fourth order tensor, then for any orthogonal transformation of the primed to the non-primed coordinates, i.e., x'_i to x_i, it transforms according to

$$c_{mnop} = \beta_{mi}\ \beta_{nj}\ \beta_{ok}\ \beta_{p\ell}\ c'_{ijk\ell} \tag{1.4}$$

where β_{ij} is the cosine of the angle between x'_i and x_j, respectively. For a rotation of angle ϕ in the x'_1 -x'_2 plane, the transformation tensor β_{ij} reduces to

$$\begin{vmatrix} \cos\phi & \sin\phi & 0 \\ -\sin\phi & \cos\phi & 0 \\ 0 & 0 & 1 \end{vmatrix} \tag{1.5}$$

which, if applied to Eq. (1.2) through the relation of Eq. (1.3) yields well known relations (see Love [38])

$$\begin{vmatrix} \sigma_{11} \\ \sigma_{22} \\ \sigma_{33} \\ \sigma_{23} \\ \sigma_{13} \\ \sigma_{12} \end{vmatrix} = \begin{vmatrix} C_{11} & C_{12} & C_{13} & 0 & 0 & C_{16} \\ C_{12} & C_{22} & C_{23} & 0 & 0 & C_{26} \\ C_{13} & C_{23} & C_{33} & 0 & 0 & C_{36} \\ 0 & 0 & 0 & C_{44} & C_{45} & 0 \\ 0 & 0 & 0 & C_{45} & C_{55} & 0 \\ C_{16} & C_{26} & C_{36} & 0 & 0 & C_{66} \end{vmatrix} \begin{vmatrix} e_{11} \\ e_{22} \\ e_{33} \\ \gamma_{23} \\ \gamma_{13} \\ \gamma_{12} \end{vmatrix} \tag{1.6}$$

where the transformation relations between the C_{pq} and C'_{pq} entries are listed in Appendix A. Notice that, no matter what rotational angle ϕ is used, the zero entries in Eq. (1.6) will remain zero. In fact, the matrix of Eq. (1.6), although particularized to orthotropic media, resembles that of monoclinic media (i.e. media which has $x_3 = 0$ as a plane of symmetry).

In terms of the rotated coordinate system x_k, we write the momentum equations as

$$\frac{\partial \sigma_{ij}}{\partial x_j} = \rho \frac{\partial^2 u_i}{\partial t^2} \tag{1.7}$$

1.2 Analysis

Substituting from Eq. (1.6) into Eq. (1.7) results in a system of three coupled equations for the displacements u_1, u_2 and u_3. If we now identify the plane of incidence to be the x_1-x_3, as in Fig. 1.1, a formal solution for the displacements u_i can be written as

$$(u_1, u_2, u_3) = (1, V, W) U e^{i\xi(x_1 + \alpha x_3 - ct)} , \tag{1.8}$$

where ξ is the wave number, c is the phase velocity ($=\omega/\xi$), ω is the circular frequency, α is still an unknown parameter, and V,W are ratios of the displacement amplitudes of u_2 and u_3 to u_1, respectively. Combinations of Eqs. (1.8), (1.7) and (1.6) yield the matrix relation

$$\begin{vmatrix} C_{11} - \rho c^2 + C_{55}\alpha^2 & C_{16} + C_{45}\alpha^2 & (C_{13} + C_{55})\alpha \\ C_{16} + C_{45}\alpha^2 & C_{66} - \rho c^2 + C_{44}\alpha^2 & (C_{36} + C_{45})\alpha \\ (C_{13} + C_{55})\alpha & (C_{36} + C_{45})\alpha & C_{55} - \rho c^2 + C_{33}\alpha^2 \end{vmatrix} \begin{vmatrix} 1 \\ V \\ W \end{vmatrix} = 0$$

Nontrivial solutions for V and W demand the vanishing of the determinant in equation (1.9) and yield an algebraic equation relating α to c. This

equation is reduced (see Appendix B) to a sixth-degree polynomial equation in α, namely

$$\alpha^6 + A_1\alpha^4 + A_2\alpha^2 + A_3 = 0 \tag{1.10}$$

Equation (1.10) admits three solutions for α^2 which we label as α_1^2, α_3^2 and α_5^2. These lead to six solutions for α which we further label as

$$\alpha_2 = -\alpha_1,\ \alpha_4 = -\alpha_3 \text{ and } \alpha = -\alpha_5 \tag{1.11}$$

Using superposition, together with the relation (1.9), we can relate the displacement ratios V_q and W_q for each α_q as

$$V_q = \frac{F_{23}(F_{11} + C_{55}\alpha_q^2) - (F_{12} + C_{45}\alpha_q^2)F_{13}}{F_{13}(F_{22} + C_{44}\alpha_q^2) - (F_{12} + C_{45}\alpha_q^2)F_{23}} \tag{1.12}$$

$$W_q = \alpha_q \frac{F_{23}(F_{11} + C_{55}\alpha_q^2) - (F_{12} + C_{45}\alpha^2)F_{13}}{(F_{12} + C_{45}\alpha_q^2)(F_{33} + C_{33}\alpha_q^2) - F_{13}F_{23}\alpha_q^2}, \quad q = 1,2\ldots6 \tag{1.13}$$

where F_{st} ,s,t= 1,2,3 are defined in Appendix B. Combining Eqs. (1.12) and (1.13) with the stress-strain relations Eq. (1.6), we rewrite the formal solutions for the displacements and stresses as

$$(u_1,u_2,u_3) = \sum_{q=1}^{6} (1, V_q, W_q)U_q\, e^{i\xi(x_1+\alpha_q x_3-ct)} \tag{1.14}$$

$$(\sigma_{33},\sigma_{13},\sigma_{23}) = \sum_{q=1}^{6} (D_{1q}, D_{2q}, D_{3q})U_q e^{i\xi(x_1+\alpha_q x_3-ct)} \tag{1.15}$$

where

$$D_{1q} = C_{13} + C_{36}\, V_q + C_{33}\, \alpha_q\, W_q \tag{1.16a}$$

$$D_{2q} = C_{55}(\alpha_q + W_q) + C_{45}\, \alpha_q\, V_q \tag{1.16b}$$

and

$$D_{3q} = -C_{45}(\alpha_q + W_q) + C_{44}\,\alpha_q V_q \quad , \; q = 1,2,\ldots,6 \tag{1.16c}$$

With reference to Eq. (1.11) and by inspection of Eqs. (1.12) - (1.16c) one deduces the relations

$$V_2 = V_1,\; V_4 = V_3,\; V_6 = V_5 \tag{1.17a}$$

$$W_2 = -W_1,\; W_4 = -W_3,\; W_6 = -W_5 \tag{1.17b}$$

$$D_{12} = D_{11},\; D_{14} = D_{13},\; D_{16} = D_{15} \tag{1.18a}$$

$$D_{22} = -D_{21},\; D_{24} = -D_{23},\; D_{26} = -D_{25} \tag{1.18b}$$

$$D_{32} = -D_{31},\; D_{34} = -D_{33},\; D_{36} = -D_{35} \tag{1.18c}$$

1.3 Derivation of reflection and transmission coefficients

To determine the reflection and transmission coefficients for plane waves incident from the fluid onto the plate surface at an arbitrary angle θ we need to obtain general solutions for the upper and lower fluids similar to those of Eqs. (1.14) and (1.15). Recognizing that the fluid does not support shear deformation, its field equations reduce to

$$\frac{\partial \sigma_{ij}^{(f)}}{\partial x_j} = \rho_f \frac{\partial u_i^{(f)}}{\partial t^2} \tag{1.19}$$

$$\sigma_{ij}^{(f)} = \lambda_f \frac{\partial u_k^{(f)}}{\partial x_k} \delta_{ij} \quad , \qquad i,j = 1,2,3, \tag{1.20}$$

where both equations hold only for i=j; ρ_f and λ_f are the fluid density and Lame' constant. If the wave is assumed to be incident and hence reflected in the upper fluid and transmitted into the lower fluid, then using similar analysis to that of the plate yields, for the upper fluid,

$$(u_1, u_2, u_3, \sigma_{33})^{(u)} = \sum_{k=1}^{2} (1, 0, W_k^{(u)}, i\xi\rho_f c^2) U_k^{(u)} e^{i\xi[x_1 + (-1)^{k+1}\alpha_f x_3 - ct]} \tag{1.21}$$

and for the lower fluid

$$(u_1,u_2,u_3,\ \sigma_{33})^{(\ell)} = (1,0,\alpha_f, i\xi\rho_f c^2)U^{(\ell)} e^{i\xi[x + \alpha_f(x_3-d)-ct]}, \quad (1.22)$$

where

$$W_1^{(u)} = \alpha_f\ ,\ W_2^{(u)} = -\alpha_f \quad (1.23a)$$

$$\alpha_f = \left(\frac{c^2}{c_f^2} - 1\right)^{\frac{1}{2}}\ ,\ c_f = \left(\frac{\lambda_f}{\rho_f}\right)^{\frac{1}{2}} \quad (1.23b)$$

Notice the vanishing of shear component u_2 in both the upper and lower fluids.

By invoking the continuity of the normal displacements and stresses at $z = 0$ and $z = d$ and setting the solid shear stresses σ_{13} and σ_{23} equal to zero at $z = 0$ and $z = d$ we obtain, for a given incident amplitude U_1^u, a system of eight linear simultaneous equations for the amplitudes $U_2^{(u)}$, U^{ℓ}, U_1, U_2, U_3, U_4, U_5 and U_6 is obtained. Solving these equations with the help of the relations (1.17) and (1.18) and applying rather lengthy algebraic reductions and manipulations, we derive the following expressions for the reflection and the transmission coefficients

$$R = \frac{U_2^{(u)}}{U_1^{(u)}} = \frac{AS-Y^2}{(S+iY)(A-iY)} \quad (1.24)$$

$$T = \frac{U^{(\ell)}}{U_1^{(u)}} = \frac{iY(S+A)}{(S+iY)(A-iY)} \quad (1.25)$$

where

$$S = D_{11}G_1\cot(\gamma\alpha_1) - D_{13}G_3\cot(\gamma\alpha_3) + D_{15}G_5\cot(\gamma\alpha_5) \quad (1.26a)$$

$$A = D_{11}G_1\tan(\gamma\alpha_1) - D_{13}G_3\tan(\gamma\alpha_3) + D_{15}G_5\tan(\gamma\alpha_5) \tag{1.26b}$$

$$Y = \frac{\rho_f c^2}{\alpha_f} \quad (W_1G_1 - W_3G_3 + W_5G_5) \tag{1.26c}$$

with

$$G_1 = D_{23}D_{35} - D_{33}D_{25} \tag{1.27a}$$

$$G_3 = D_{21}D_{35} - D_{31}D_{25} \tag{1.27b}$$

$$G_5 = D_{21}D_{33} - D_{31}D_{23} \tag{1.27c}$$

$$\gamma = \xi d/2 = \omega d/2c. \tag{1.27d}$$

1.4 Results and discussions

Except for the more complicated definitions of the functions S,A and Y, the expressions R and T resemble those reported in our earlier paper [34], and our notation was chosen for consistency with this previous calculation.

The expressions of Eqs. (1.24) and (1.25) for the reflection and the transmission coefficients contain, as a by-product, the characteristic equation for the propagation of modified (leaky) guided waves in the plate. We refer to such waves as plate waves [34] rather than Lamb waves, whose properties were derived originally by Lamb [39] for isotropic solids in the absence of the fluid. Setting either denominator equal to zero, namely

$$(S+iY)\ (A-iY) = 0 \tag{1.28}$$

defines the characteristic equations for such waves, where the vanishing of the first term corresponds to symmetric and the second to antisymmetric mode propagation. In the absence of the fluid, i.e. for ρ_f(or Y) = 0, Eqs. (1.28) reduce to SA = 0 which is the characteristic equation for Lamb-like waves in the orthotropic plate.

For the special cases of propagation along axes of symmetry (in the present example $\phi = 0°$ or $90°$), the off-diagonal tensor components C_{16}, C_{26}, C_{36}, and C_{45} vanish in Eq. (1.6). The implication is that the displacements u_2, out of the x_1-x_3 plane, go to zero, thereby confining all particle motion to the plane of incidence. This result is equivalent to the decoupling of the wave equations for vertical and horizontal shear motions in the plate, noted by us and other authors in treating anisotropic plates [23,34]. In addition, the secular equation (1.10) for the x_3-component of the wavevector factors and reduces to the lower dimensional result presented in our earlier analysis [33,34]. In fact, for symmetry axis propagation we recover entirely our previous results for the reflection coefficient from the fluid-coupled composite plate.

In comparisons between the results of many measurements at several azimuthal angles and the model calculation, we have concentrated our attention, as in previous investigations [33,34], on the reflection coefficient. Since the basis of the experimental data is an amplitude signal in the reflected field of the incident beam, we calculate the plane-wave reflection coefficient for the plate and investigate it for the same type of behavior as we observe in the measurements. In addition to direct comparisons of amplitude spectra, we have also expressed our results as dispersion-like curves, where the results correspond to functions conditioned by the reflection coefficient. The theoretical dispersion curves are based on the occurrence of total transmission for given Fd and incident angle. Numerically, the curves are generated by searching Eq. (1.24) for the minima in the magnitude of the reflection coefficient which

are accompanied by a rapid reversal in its phase. Both of these aspects of our studies are presented below.

A finite ultrasonic beam is composed of a range of plane wave components which define its angular spread,

$$\beta(x) = \int \hat{\beta}(\xi)\exp(-2\pi i\xi x)d\xi \qquad (1.29)$$

where $\beta(x)$ is the one-dimensional real space incident beam profile, x is a coordinate perpendicular to the beam direction, and the caret denotes Fourier transform. When such a finite beam interacts with a plate, each Fourier component of the incident field will contribute to the reflected field, weighted by the appropriate value of the reflection coefficient for that ξ. The resulting expression for the reflected field is given by

$$A(Fd,x_i) = \int\hat{\beta}(\xi)R(\xi,Fd)\exp[-2\pi i\xi(x_1-\alpha_f x_3)]d\xi \qquad (1.30)$$

where $R(\xi,Fd)$ is the reflection coefficient from Eq. (1.24) for the composite plate. The expression of Eq. (1.30) evaluated over frequency is an approximation to the experimental spectrum of the plate, if the beam profile $\beta(x)$ is chosen to represent the incident beam. We have performed such calculations for a variety of experimental conditions. Some typical comparisons are contained in Figs. 1.2(a)-(d).

Figure 1.2(a) shows the measured and predicted spectra from 1 to 8 MHz for an incident angle $\theta = 12^0$ and azimuthal angle $\phi = 30^0$. The two curves have been vertically scaled, but in no other way adjusted. The solid curve is the expression of Eq. (1.30), and the dashed curve is the experimental data deconvolved to remove transducer response. Positions of the deep minima in the two curves are nearly coincident, as we have observed for propagation in the fiber direction [34]. We conjecture that the additional shallower sharp dips, some of which do not appear in the data, arise from

the coupling between vertical and horizontal shear displacements which occurs for propagation in a general azimuthal direction. At $\theta = 28^0$ and $\phi = 15^0$ in Fig. 1.2(b), similar results are found, where the general trend of the data is well reproduced by the model calculation. In particular, the two shallower minima between 2 and 4 MHz are given fairly accurately by the prediction. This structure disappears for $\phi = 0^0$, leaving only the deep minima at 1.9, 4.3 MHz, and beyond. Holding the incident angle constant and incrementing ϕ to 30^0, the structure of the curve has evolved in Fig. 1.2(c) with the two minima near 3 MHz approaching each other more closely and deepening considerably. These features are also seen in the model calculations. In the final frame, Fig. 1.2(d), results are given for $\theta = 24^0$ and $\phi = 90^0$. This case corresponds to symmetry axis propagation, and therefore the complex structure of the previous examples is largely absent. The positions of the minima are well modeled by the theory, whereas the minor differences in the lineshape details may be attributed to wavefront distortion and sound absorption, neither of which is considered in the model.

Taking the results of the many dozens of Cmimenti's experimental spectra such as those shown in Fig. 1.2 and recording the minima as a function of the incident angle (expressed through Snell's law as a phase velocity), yields a dispersion-like plot of the ultrasonic reflection behavior. In previous work [34,41] we demonstrated that the hypothesis of Cremer [42] concerning the coincidence of reflection minima with the excitation of Lamb wave modes is not well satisfied in all regions of plate wave dispersion in graphite-epoxy composites. Therefore, although we present these data in the manner of a velocity dispersion curve, it must be stressed that it is the reflection properties which are being reported.

Figure 1.3(a) shows data acquired in the current study at an azimuthal angle $\phi = 0^0$ plotted together with the results of the analytical prediction derived by examining the behavior of the reflection coefficient, Eq. (1.24). To obtain the theory curves rapid phase variations in the reflection coefficient, generally indicative of total transmission, have been recorded as a function of Fd for many values of phase velocity. These calculations are presented as small filled circles which coalesce into solid curves over most of the plot. In some cases to be discussed a dashed line has been added as a guide to the eye. In Fig. 1.3(a) the data, plotted as discrete crosses, are in excellent agreement with the prediction of our new, more general model. All features of the data from $\theta = 12^0$ to $\theta = 40^0$ are well explained in the model. Propagation in the other material symmetry direction $\phi = 90^0$ is shown in Figure 1.3(b). Here the results reflect the substantial effective softening of the composite as the fiber axis is rotated out of the plane of incidence. Therefore, we observe a marked reduction in the phase velocities at which certain features occur. The vertical intercept of the curve, which is similar to the S_0 mode, is seen to be near $c_p = 2.2$ km/sec. Likewise, the point of diminishing slope of some of the higher order curves is much lower here than for $\phi = 0^0$ as in Fig. 1.3(a). In fact, the behavior referred to is not even visible in Fig. 1.3(a) because it occurs above $c_p = 9.8$ km/sec.

For a transversely isotropic material, setting $\phi = 90^0$ implies that elastic behavior in the plane of the incidence ($x_2' - x_3'$ plane) will be isotropic. An important experimental finding by Chementi of the present study is the suggestion that transverse isotropy is not an appropriate symmetry class for the eight-ply Thornel/Ciba-Geigy composite sample we

studied. Our result on the inequality of C'_{22} and C'_{33} stands in contrast to previous investigations, both mechanical [43] and ultrasonic [44], on thick-section T300 - 5208 unidirectional composite. In these earlier studies the ratio C'_{22}/C'_{33} was measured to be within 2% of unity. Because of the method of fabrication of these materials in which compressive stresses are exerted on the surfaces of the curing composite, fibers might tend to be distributed nonuniformly in the plate. That is, the number of fibers per unit length in the x'_3 direction could be higher than the same quantity in the x'_2 direction (refer to Eqs. (1.1)-(1.3)). Our experimental data for $\phi = 90^0$ are consistent with the above interpretation and draw us to the conclusion that orthotropy is the correct symmetry class for thin sections of this material. Since the elastic constant denoted C'_{22} in Eq. (1.3) is difficult to measure independently, we have inferred this quantity from our reflection data and the model calculation. The results of this evaluation yield a ratio of C'_{22} to C'_{33} of 0.72. Once this adjustment in C'_{22} is made, all subsequent comparisons at intermediate values of ϕ are carried out using this same constant. Here we note that C'_{22} does not influence the propagation behavior along $\phi = 0^0$, and hence this issue was not encountered in our previous work [34]. In our calculations we use the qraphite- epoxy material properties listed in Ref. [40].

If we now depart from the principal axis directions, the reflection behavior becomes substantially more complicated, as can be seen in Fig. 1.4(a) for $\phi = 30^0$. The simple structure of Fig. 1.3(a) is replaced by curves which split apart, rejoin, and cross over each other. Throughout the range of the measurements, relatively good agreement with the theory is

apparent. Although interpretation of these results is delicate, we may note a few consistent trends. As the fiber direction is rotated out of the plane of incidence, the effective material constants begin to soften, causing the phase velocity intercept of the S_0-like curve to decrease, as in Fig. 1.3(b). In Fig. 1.4(a) that velocity is about 8.5 km/sec, whereas the value is 9.8 km/sec for propagation along the fibers. Moreover, an additional set of curves seems to have nucleated, in agreement with our calculations and data starting as low as $\phi = 15^0$. These general features will be seen to persist in the results for higher values of ϕ as well.

Comparison of measurement and theory for $\phi = 45^0$ is contained in Fig. 1.4(b). As expected, the intercept velocity has decreased to about 7 km/sec, and behavior of even higher complexity has appeared above this value. The series continues with $\phi = 60^0$ in Fig. 1.4(c), where the overall pattern established earlier is evident here also. Finally, in Fig. 1.4(d) for $\phi = 75^0$ we have the last of the comparisons. The intercept velocity here is near 3.4 km/sec, nearly a factor of 3 below its $\phi = 0^0$ value. These curves contain an almost unbelievably rich variety of reflection phenomena, considering the relatively simple form of the $\phi = 0^0$ curves in Fig. 1.2(a). As we have stated earlier, it is our conjecture that these additional features arise from the coupling of the vertically and horizontally polarized waves, which are independent for propagation along principal axes. We note in closing this section that in all these comparisons, but especially Figs. 1.4(c) and 1.4(d), agreement between measurements and theory is not simply a matter of general trends. Excellent detailed agreement is seen over most of these plots, in spite of the richly complex behavior observed for a general azimuthal angle. This observation lends confidence in the validity of the theoretical approach.

1.5 Free waves in monoclinic plates

In a recent paper [45], we developed the analysis for the propagation of free waves in a general anisotropic plate and presented numerical results for some special cases of interest. We began with a formal analysis for waves in a plate belonging to the triclinic symmetry group (the most general with 21 independent elastic constants). The calculation was then carried forward for the slightly more specialized case of a monoclinic plate (13 independent elastic constants), where the surface of the plate is parallel with the single plane of mirror symmetry in this material system. We derived the secular equation for this case in closed form and isolated the mathematical conditions for symmetric and antisymmetric wave mode propagation in completely separate terms. Material systems of higher symmetry, such as orthotropic, transversely isotropic, cubic, and isotropic are contained implicitly in our analysis. The equivalent crystal systems of monoclinic, orthorhombic, hexagonal and cubic may be substituted for the elastic material systems analyzed here. We demonstrated numerical free wave dispersion results drawn from concrete examples of materials belonging to several of these symmetry groups. For orthotropic and higher symmetry materials where the remaining two principal axes lie in the plane of the plate, it was shown that the particle motions for Lamb and SH modes uncouple if propagation occurs along either of these in-plane axes.

1.6 The case of a plate seperating a liquid from a vacuum

In another recent paper [46] we derived an exact expression for the reflection coefficient of an orthotropic plate, which is loaded on a single surface by a fluid medium while the second surface is stress free. For this case, we assumed guided wave propagation along a principal axis in the plate. We found that the reflection coefficient for this case can be

expressed in terms which are identical to the case of a fully immersed plate, namely expressions (1.26) and (1.27) . Furthermore, it bears a strong formal resemblance to the reflection coefficient of the fluid-coupled halfspace, in particular as far as the role of the fluid is concerned. From the results derived we obtained the solution for an isotropic plate to compare with experiments.

2. BIAXIALLY LAMINATED COMPOSITE PLATES

This section presents the analysis of biaxially laminated plates utilizing water as a fluid coupling medium. Here the stacking sequence of the individual laminae is restricted such that in each layer a principal material axis lies in the incident plane of the acoustic wave. In what follows we shall use the transfer matrix approach to derive our results. Specifically we derive the reflection and transmission coefficients from which the characteristic behavior of the system is identified. Results are presented both as reflection spectra and dispersion curves. In general, very good agreement is found between prediction and experiment. Moreover, significant changes in the reflection spectra are observed, depending on the layer ordering in the composite plates. In the next section we summarize the theoretical calculation, followed by a comparison with the concurrently acquired experimental date of Chimenti.

2.1 Analysis

Consider a plate consisting of an arbitrary number n of monoclinic layers rigidly bonded at their interfaces and stacked normal to the x_3 direction of a cartesian system $x_i = (x_1, x_2, x_3)$. Hence the plane of each layer is parallel to the x_1-x_2 plane which is also chosen to coincide with the bottom surface of the laminated plate. The stacking of the layers is restricted, however, such that the x_1 and x_2 directions coincide with their principal axes. Thus, for a plate constructed from several uniaxial fibrous composite lamina of the same material, only 0° and 90° lay-ups are allowed. In this section, we derive exact analytical expressions for the reflected and transmitted fields of an acoustic wave incident from a surrounding fluid

onto the plate. The wave is restricted to propagate along one of the in-plane symmetry axes of the plate. Sufficient generality is maintained such that the solutions obtained will include, as special cases, those pertaining to higher symmetry materials.

Using our homogeneous, monoclinic plate analysis as a starting point we introduce, for each layer k, a local coordinate system $x_i^{(k)}$ with origin at the interface between layers k-1 and k. Hence layer k occupies the space $0 \leq x_3^{(k)} \leq d^{(k)}$ where $d^{(k)}$ is its thickness. Thus the laminated plate has total thickness $d = \sum_{k=1}^{n} d^{(k)}$.

With this choice of coordinate system and the restricted propagation directions mentioned above, the displacement will reduce to a two-dimensional vector. In-plane transverse motion will vanish, and the remaining field variables will be independent of x_2. The relevant field equations for each layer will thus consist of

$$\sigma_{ij,j} = \rho u_i \qquad i,j = 1,3 \tag{2.1}$$

and the constitutive relations

$$\sigma_{ij} = c_{ijk\ell} e_{k\ell} \quad , \tag{2.2}$$

appropriately specialized to the two-dimensional case of propagation in the x_1-x_3 plane. Appropriate field equations for the fluids can be similarly written by noting that fluids are isotropic and cannot support shear deformation.

The field equations in the solid and fluid media must be supplemented with the appropriate interfacial continuity conditions. At the fluid-plate interface, $x_3 = 0$ and $x_3 = d$, the appropriate continuity conditions are

$$\sigma_{13} = 0,\ \sigma_{33} = \sigma_{33}^{(f)}\ ,\ u_3 = u_3^{(f)}\ , \tag{2.3}$$

whereas at the lamina interfaces they are

$$u_1^{(k)} = u_1^{(k+1)}\ ,\ u_3^{(k)} = u_3^{(k+1)}\ ,\ \sigma_{33}^{(k)} = \sigma_{33}^{(k+1)}\ ,\ \sigma_{13}^{(k)} = \sigma_{13}^{(k+1)}\ . \tag{2.4}$$

In what follows we shall describe the propagation process in the system. For each layer k, equations (2.1) - (2.2) are combined into two coupled equations in u_1 and u_3 and a formal solution in the form

$$(u_1,u_3) = (U,W)e^{i\xi(x_1+\alpha x_3-ct)} \tag{2.5}$$

where U and W are displacement amplitudes, ξ is the x_1 wave number, c is the phase velocity and α is the ratio of the x_3 and x_1 wave numbers. For nontrivial solutions, one obtains a characteristic equation for α. This equation admits four solutions and, by using superposition, one finally obtains

$$(u_1,u_3,\bar{\sigma}_{33},\bar{\sigma}_{13}) = \sum_{p=1}^{4} (1,W_p,D_{1p},D_{2p})_k U_p e^{i\xi(x_1+\alpha_p x_3-ct)}\ , \tag{2.6}$$

where the index p assumes the values 1,2,3,4 and α is the solution of

$$A\alpha^4 + B\alpha^2 + C = 0 \tag{2.7}$$

with

$$A = C_{33}C_{55}\ ,$$

$$B = (C_{11} - \rho c^2)C_{33} + (C_{55} - \rho c^2)C_{55} - (C_{13} + C_{55})^2\ ,$$

$$C = (C_{11} - \rho c^2)(C_{55} - \rho c^2)\ ,$$

and, for each α_p

$$W_p = \frac{\rho c^2 - C_{11} - C_{55}\alpha_p^2}{(C_{13} + C_{55})\alpha_p}\ ,$$

$$D_{1p} = C_{13} + C_{33}\alpha_p W_p \quad ,$$

$$D_{2p} = C_{55}(\alpha_p + W_p) \quad , \quad \bar{\sigma}_{ij} = \sigma_{ij}/i\xi \quad . \tag{2.8}$$

Equation (2.6) can be used to relate the displacements and stresses at $x_3^{(k)} = 0$ to those at $x_3^{(k)} = d^{(k)}$. This can be done by specializing (2.6) to $x_3^{(k)} = 0$ and to $x_3^{(k)} = d^{(k)}$, and eliminating the common amplitude column made up of U_1, U_2, U_3, and U_4 resulting in

$$(F_i)_{x_3^{(k)} = d^{(k)}} - [a_{ij}]_k (F_j)_{x_3^{(k)} = 0} \quad , \tag{2.9}$$

here F_i, for i = 1,2,3, and 4, designates the field variables $u_1, u_3, \bar{\sigma}_{33}$, $\bar{\sigma}_{13}$, respectively. Here the summation convention on repeated indices i and j hold and

$$[a_{ij}]_k = \begin{bmatrix} B_1 & B_2 & B_3 & B_4 \\ W_1B_1 & W_2B_2 & W_3B_3 & W_4B_4 \\ D_{11}B_1 & D_{12}B_2 & D_{13}B_3 & D_{14}D_4 \\ D_{12}B_1 & D_{22}B_2 & D_{23}B_3 & D_{24}B_3 \end{bmatrix}_k \begin{bmatrix} 1 & 1 & 1 & 1 \\ W_1 & W_2 & W_3 & W_4 \\ D_{11} & D_{12} & D_{13} & D_{14} \\ D_{21} & D_{22} & D_{23} & D_{14} \end{bmatrix}^{-1}_k \tag{2.10a}$$

and

$$B_p = e^{i\xi\alpha_p d} \quad , \quad p = 1,2,3,4 \tag{2.10b}$$

By applying the above procedure for each layer and invoking the continuity relations (2.4) at the layer interfaces we can finally relate the displacements and stresses at the top of the layered plate to those at its bottom via the transfer matrix multiplications [37]

$$[A_{ij}] = [a_{ij}]_n [a_{ij}]_{n-1} \cdots [a_{ij}]_1 \tag{2.11a}$$

resulting in

$$(F_i)_{x_3-d} = [A_{ij}](F_j)_{x_3-0} \tag{2.11b}$$

2.2 Derivation of reflection and transmission coefficients

Now, in order to satisfy the remaining continuity conditions (2.3) at the plate-fluid interfaces, we need to solve the field equations in the fluid. By inspection, such solutions can be deduced from the formal solution (2.6). First, due to the absence of shear deformation, specializing (2.6) to the upper fluid half-space yields

$$\begin{bmatrix} u_1^{(u)} \\ u_3^{(u)} \\ \bar{\sigma}_{33}^{(u)} \end{bmatrix} = \begin{bmatrix} 1 & 1 \\ \alpha_f & -\alpha_f \\ \rho_f c^2 & \rho_f c^2 \end{bmatrix} \begin{bmatrix} U_1^{(u)} e^{i\xi\alpha_f(x_3-d)} \\ U_2^{(u)} e^{-i\xi\alpha_f(x_3-d)} \end{bmatrix} e^{i\xi(x_1 - ct)} \tag{12a}$$

where

$$\alpha_f^2 = (c^2/c_f^2) - 1, \quad \bar{\sigma}_{33}^{(u)} = \sigma_{33}^{(u)}/i\xi \tag{2.12b}$$

Here, $U_1^{(u)}$ is the constant amplitude of the incoming wave and $U_2^{(u)}$ is that of the reflected wave. Also, the sub and superscripts u denote quantities belonging to the upper fluid. Similarly, for the lower fluid the response can be obtained by analogy with the upper fluid's response given by (2.12a) and by concurrently satisfying the requirement for bounded solutions so that

$$\begin{bmatrix} u_1^{(\ell)} \\ u_3^{(\ell)} \\ \bar{\sigma}_{33}^{(\ell)} \end{bmatrix} = \begin{bmatrix} 1 \\ \alpha_f \\ \rho_f c^2 \end{bmatrix} U_1^{(b)} e^{i\xi(x_1 + \alpha_f x_3 - ct)} , \tag{2.13}$$

where ℓ denotes the lower fluid.

Subjecting the solutions (2.12a), (2.13) and (2.6) to the continuity conditions (2.3) while identifying the superscript (f) with (u) and (ℓ) at $x_3 = d$ and $x_3 = 0$, respectively finally yields the reflection and transmission coefficients

$$R = \frac{M_{21} + QM_{22} - Q(M_{11} + QM_{12})}{M_{21} + QM_{22} + Q(M_{11} + QM_{12})} \tag{2.14a}$$

$$T = \frac{2QM_{21}}{M_{21} + QM_{22} + Q(M_{11} + QM_{12})} , \tag{2.14b}$$

where

$$Q = \frac{\rho_f c^2}{\alpha_f} , \tag{2.15a}$$

$$\begin{bmatrix} M_{11} & M_{12} \\ M_{21} & M_{22} \end{bmatrix} = \begin{bmatrix} A_{21} & A_{22} & A_{23} \\ A_{31} & A_{32} & A_{33} \end{bmatrix} \begin{bmatrix} -A_{42} & -A_{43} \\ A_{41} & 0 \\ 0 & A_{41} \end{bmatrix} . \tag{2.15b}$$

2.3 Results and discussions

Since ultrasonic reflection behavior in biaxial composites is dependent on details of the layering, we present our results primarily as frequency spectra from which dispersion curves could be developed. An example of experimental and theoretical curves for a four-layer biaxial composite $[0_2, 90_2]_s$ (pictures of which are shown in Fig.2.1) are depicted in Fig. 2.2. The dashed curve is the measurement, while the calculation is demonstrated as a solid curve. Only the relative amplitudes of the two curves have been scaled, since absolute reflectance has not been measured. An incident angle of 16° is selected, and the fiber direction in the upper

layer is in the incident plane. The comparison between experiment and theory is very good; nearly all details of the data are reproduced by the calculation.

Figure 2.3 shows the result of rotating the incident plane by 90° while maintaining a 16° incident angle, so that the upper fiber layer is perpendicular to the wave propagation direction. The experimental reflection spectrum is markedly different, both in appearance and precise location of the minima. Yet the model calculation follows the data very well. This case, and many others we have examined, exemplify the complexity and non-intuitive nature of the results in layered anisotropic materials. Clearly, a simpler model in which the mechanical properties are averaged through the plate thickness would be unable to account for the difference between the data in Figs. 2.2 and 2.3. A further comparison at an incident angle of 20° is shown in Fig. 2.4. The solid curve is theory, and the dashed curve is the normalized data for the $[0_2,90_2]_s$ sample with the top layer fibers in the incident plane. Once again good agreement is observed in this direct comparison. Rotation of the incident plane through 90° demonstrates a similar strong variation of the reflection spectrum, as seen in Fig. 2.5. No minimum in Fig. 2.5 coincides with one from Fig. 2.4. The structure of the curve is completely different, but the agreement between measurement and prediction is still very good. In Fig. 2.5 we see that the theory curve has sharper features than the data, as expected for the plane-wave reflection coefficient.

A much more complicated situation is presented by a 12-ply sample having an alternating structure in each layer. The lay-up scheme is $[0,90]_{3s}$. No

special care has been taken in the preparation of this sample or the other biaxial lay-up, and therefore some discrepancies between data and prediction can be attributed to this source. However, even with this proviso the significant features of the experimental data are well reproduced by the theory curves. Figure 2.6 shows measurements for an incident angle of 22° with the upper layer fiber direction in the incident plane. In Fig. 2.7 the incident plane is rotated 90°. Comparison of these two cases reveals that even with as many as 12 alternating layers, the order of the anisotropic layers is still important. The minima near 1 and 2 MHz are basically constant between Figs. 2.6 and 2.7, but significant differences in the successive structure of the curve minima occur above 2 MHz. These variations can be attributed only to the order of layering, a relatively surprising result since only the slow transverse quarter wavelength in the 90-degree layers is approaching the layer thickness.

At an incident angle of 30° with $\phi=0^{\circ}$ in Fig. 2.8 comparable results are achieved, where the theory curve follows the data rather closely, except near 4 MHz. The small amplitude oscillations on the peaks of the experimental curve at 3.5 and 4.8 MHz are artifacts which have been caused by overlap reflections from the water surface in the tank. In Fig. 2.9 with the fiber direction perpendicular to the incident plane the curve structure below 2.2 MHz repeats that of Fig. 2.8, but substantial differences in the reflected field amplitude appear at higher frequency values, as in the previous spectrum pair for $\theta=22^{\circ}$.

For the case of the biaxially laminated composite samples, dispersion behavior is clearly structure-dependent. However, by way of illustration we

present experimental and theoretical dispersion curves for the $[0_2,90_2]_s$ plate in the $\phi=90^\circ$ direction in Fig. 2.10, where the phase velocity has been inferred from the incident angle. We have shown previously [33,34] that in low density materials like graphite-epoxy composites reflection-derived dispersion curves can deviate significantly from solutions of the characteristic equation contained implicitly in Eq. (2.14a). Evidence of that deviation can be seen in the data (open circles) and theory (solid line) in the lower left portion of Fig. 2.10, where the lowest order mode appears to turn back on itself. In general, agreement between measurement and calculation is good, as expected on the basis of the comparisons presented for reflection spectra in Figs. 2.2-2.9. However, it should be emphasized that the curves in Fig. 2.8 are not universal; that is, they are dependent not only on the elastic properties of graphite-epoxy. If the laminate structure or layer ordering changes, the dispersion behavior will vary accordingly.

3. MULTILAYERED ANISOTROPIC PLATES

In this section we generalize the results of both of our earlier sections to the case of a plate consisting of an arbitrary number of arbitrarily oriented anisotrpic layers. Each of the individual layers is allowed to possess up to as low as monoclinic symmetry. The plate is assumed to be immersed in a fluid and subjected to incident acoustic waves at arbitrary angles from the normal as well as at arbitrary azimuthal angles. Solutions are obtained for the individual layers which relate the field variables at the upper and lower layer surfaces. The response of the total plate proceeds by employing the matrix transfer method [37] which require satisfying appropriate interfacial conditions across the layers. The reflection and transmission coefficients of the total system will are derived from which all of the propagation characteristics are readily extracted. Our results are rather general and contain a wide variety of special cases.

3.1 Analysis

Consider a plate consisting of an arbitrary number n of anisotropic layers, each possessing up to as low as monoclinic symmetry, rigidly bonded at their interfaces and stacked normal to the x_3 axis of a global orthogonal Cartesian system $x_i = (x_1, x_2, x_3)$. Hence the plane of each layer is parallel to the x_1-x_2 plane which is also chosen to coincide with the bottom surface of the layered plate. To maintain generality we shall assume each layer be arbitrarily oriented in the x_1-x_2 plane. In order to be able to describe the relative orientation of the layers we shall assign for each

layer k, k = 1,2,...,n, a local cartesian coordinate $(x_i')_k$ such that its origin is located in the middle plane of the layer with $(x_3')_k$ normal to it. Thus, layer k extends from $-d^{(k)}/2 \leq (x_3')_k \leq d^{(k)}/2$ where $d^{(k)}$ is its thickness. According to this notation the total thickness of the layered plate d equals the sum of the thicknesses of its layers, and hence the plate occupies the region $0 \leq x_3 \leq d$. Equivalently, the orientation of the kth layer in the x_i space can be described by a rotation of an angle ϕ_k between $(x_1')_k$ and x_1. With this , once all orientation angles ϕ_k are specified the geometry of the plate will be defined.

Without any loss in generality we shall assume that a plane wave is incident in the x_1-x_3 plane on the plate from the upper fluid at an arbitrary angle. The problem here is to study the reflected and transmitted fields. We therefore conduct our analysis in a coordinate system formed by incident and reflected planes rather than by material symmetry axes. Accordingly, the primed system $(x_i')_k$ rotates with one material symmetry axes while the global unprimed system x_i remains invariant. As was pointed out in the introduction this approach leads to significant simplification in our algebraic analysis and computations.

In what follows we use the analytical procedure of section 1 in order to construct a transfer matrix for each layer k. This matrix relates the displacements $(u_i)_k$ and stresses $(\sigma_{ij})_k$ of one face to those of the other of layer k. Using our earlier analytical procedure, the formal solutions for each layer can be adapted from equations (1.14) and (1.15) which hold for

each layer and can be used to relate the displacements and stresses at $(x_3')_k = -d^{(k)}/2$ to those at $(x_3')_k = d^{(k)}/2$. This can be done by specializing these equations to these two locations, eliminating the common amplitudes $U_1,\ldots,U_6$ and after rather lengthy algebraic reductions and manipulations we obtain (with the summation holding)

$$F_p^+ = a_{pq}F_q^- \quad , \; p,q = 1,2,\ldots,6 \tag{3.1}$$

where $F_p^{\pm}$ stand for the variables column $[u_1,u_2,u_3,\sigma_{33},\sigma_{13},\sigma_{23}]_{\pm}^T$ specialized to the upper and lower surfaces of the layer, k, respectively, and

$$[a_{pq}]_k = [T_{ps}B_{sq}]_k \tag{3.2}$$

where

$$T_{ps} = \begin{vmatrix} 1 & i & 1 & i & 1 & i \\ V_1 & iV_1 & V_3 & iV_3 & V_5 & iV_5 \\ iW_1T_1 & W_1T_1' & iW_3T_3 & W_3T_3' & iW_5T_5 & W_5T_5' \\ D_{11} & iD_{11} & D_{13} & iD_{13} & D_{15} & iD_{15} \\ iD_{21}T_1 & D_{21}T_1' & iD_{23}T_3 & D_{23}T_3' & iD_{25}T_5 & D_{25}T_5' \\ iD_{31}T_1 & D_{31}T_1' & iD_{33}T_3 & D_{33}T_3' & iD_{35}T_5 & D_{35}T_5' \end{vmatrix} \tag{3.3}$$

Here, B_{sq} is obtained from the above matrix T_{ps} by replacing i by -i as it explicitly appears and inverting the resulting matrix in Eq. (3.3)

$$T_r' = T_r^{-1} = \cot(\xi\alpha_r d/2^{(k)}) \quad , \quad r = 1,3,5 \tag{3.4}$$

The matrix $[a_{pq}]_k$ constitutes the most general transfer matrix for the orthotropic layer k. It allows the wave to be incident on layer k at an arbitrary angle from the normal x_3 or equivalently $(x_3')_k$ and at any azimuthal angle ϕ. Matrix transfer for higher symmetry material such as transversely isotropic, cubic and isotropic can be obtained from Eq. (3.2) as asymptotically limiting cases. Furthermore, if the wave happens to propagate along an in-plane axis of symmetry of layer k (namely for $\phi_k = 0°$ or 90°) results for such a case can be obtained from (3.2) in the limit. Strictly speaking Eq. (3.2) does not hold in its present form if ϕ_k is identically 0° or 90°. This is of course due to the presence of the superflous coupling (as implied by Eq. (3.1)) between the equations describing the horizontally polarized wave (SH) and the Lamb wave. The matrix transfer technique then yields, via the continuity of displacements and stresses at the various layer interfaces, the response vector at $x_3 = d$ in terms of the response vector at $x_3 = 0$

$$F_p(d) = A_{pq}\, F_q(0) \tag{3.5}$$

where

$$[A_{pq}] = [a_{pj}]_n\, [a_{jk}]_{n-1} \cdots [a_{rq}]_1 \,. \tag{3.6}$$

Using superposition and the stress-strain relations (6) we finally obtain the formal solutions

3.2 Top Fluid Boundary

The plate we consider separates a top fluid half-space from the bottom bounding media. To maintain generality we here consider a different fluid or a vacuum as choices for the bottom bounding medium. The input wave is assumed to be originating in the top fluid half-space and incident on the plate at an arbitrary angle from the normal. The displacements and stresses

within the top fluid are given by properly specializing (1.14) and (1.15) and recognizing the absence of shear deformation within the fluid so that

$$\begin{vmatrix} u^{(u)} \\ w^{(u)} \\ \dot{\sigma}_z^{(u)} \end{vmatrix} = \begin{vmatrix} 1 & 1 \\ \alpha_u & -\alpha_u \\ \rho_u c^2 & \rho_u c^2 \end{vmatrix} \begin{vmatrix} U_1^{(u)} e^{iq\alpha_u(z_3-d)} \\ U_2^{(u)} e^{-iq\alpha_u(z_3-d)} \end{vmatrix} e^{i\xi(x-ct)} \tag{3.7}$$

where $\alpha_u^2 = (c^2/c_u^2) - 1$, $U_1^{(u)}$ is the constant amplitude of the incoming wave, $U_2^{(u)}$ is that of the reflected wave and the sub and superscripts u denote quantities belonging to the fluid. The continuity conditions at the plate-fluid interface are given by

$$w^{(u)} = w^{(n)} \ , \ \sigma_{33}^{(u)} = \sigma_{33}^{(n)} \ , \ \sigma_{13}^{(n)} = \sigma_{23}^{(n)} = 0 \ , \text{ at } x_3 = d. \tag{3.8}$$

3.3 Bottom Bounding Fluid

If the bottom bounding medium of the plate consists of a different fluid, then its formal solution consists of the transmitted component and is given by

$$\begin{vmatrix} u^{(b)} \\ w^{(b)} \\ \dot{\sigma}_z^{(b)} \end{vmatrix} = \begin{vmatrix} 1 \\ \alpha_b \\ \rho_b c^2 \end{vmatrix} U_1^{(b)} e^{i\xi(x_1-ct+\alpha_b x_3)} \tag{3.9}$$

With this, the appropriate interface conditions at the bottom of the plate are

$$w^{(1)} = w^{(b)} \ , \ \sigma_{33}^{(1)} = \sigma_{33}^{(b)} \ , \ \sigma_{13}^{(1)} = \sigma_{23}^{(1)} = 0 \ , \text{ at } x_3 = 0. \tag{3.10}$$

Combinations of Eqs. (3.7) and (3.10) yield the following expressions for reflection and transmission coefficients

$$R = \frac{(M_{21} + Q_b M_{22}) - Q_u(M_{11} + Q_b M_{12})}{(M_{21} + Q_b M_{22}) + Q_u(M_{11} + Q_b M_{12})} \tag{3.11a}$$

$$T = \frac{2Q_b(A_{51}A_{62} - A_{61}A_{52})}{(M_{21} + Q_b M_{22}) + Q_u(M_{11} + Q_b M_{12})} \tag{3.11b}$$

where

$$M_{11} = \det \begin{vmatrix} A_{31} & A_{32} & A_{33} \\ A_{51} & A_{52} & A_{53} \\ A_{61} & A_{62} & A_{63} \end{vmatrix} \quad , \quad M_{12} = \det \begin{vmatrix} A_{31} & A_{32} & A_{34} \\ A_{51} & A_{52} & A_{54} \\ A_{61} & A_{62} & A_{64} \end{vmatrix} \tag{3.12a}$$

$$M_{21} = \det \begin{vmatrix} A_{41} & A_{42} & A_{43} \\ A_{51} & A_{52} & A_{53} \\ A_{61} & A_{62} & A_{63} \end{vmatrix} \quad , \quad M_{22} = \det \begin{vmatrix} A_{41} & A_{42} & A_{44} \\ A_{51} & A_{52} & A_{54} \\ A_{61} & A_{62} & A_{64} \end{vmatrix} \tag{3.12b}$$

and

$$Q_u = \frac{\rho_u c^2}{\alpha_u} \quad , \quad Q_b = \frac{\rho_b c^2}{\alpha_b} \tag{3.12c}$$

The results pertaining to the bottom free conditions (i.e., the absence of a bottom bounding media, in essence a vacuum) can be easily obtained from those corresponding to the above case of a different fluid bounding media by setting $Q_b = 0$. This results in

$$R = \frac{M_{21} - Q_u M_{11}}{M_{21} + Q_u M_{11}} \tag{3.13a}$$

$$T = 0 \tag{3.13b}$$

as expected.

3.4 Qualitative description of results

So far we have derived expressions for the reflection and transmission coefficients for multilayered plates consisting of an arbitrary number of anisotropic layers. Specifically, equations (3.11) and (3.13) list results obtained for such plates bounded by an upper fluid and whose bottom bounding medium consists of either a different fluid or a vacuum , respectively. Results for propagation along axes of symmetry can be obtained asymptotically from the general results. The expressions (3.11) and (3.13) for the reflection and transmission coefficients contain, as a by-product, the characteristic equation for the propagation of modified (leaky) free

waves on the corresponding media. The vanishing of the denominator in Eq. (3.11), namely,

$$(M_{21} + Q_b M_{22}) + Q_u(M_{11} + Q_b M_{12}) = 0 \tag{3.14}$$

defines the characteristic equation for such waves on a plate separating two different fluids. By setting $\rho_b = \rho_u$ we get results for the free waves on orthotropic plates immersed in a single fluid. Furthermore, in the absence of both fluids Eq. (3.14) reduces to

$$M_{21} = 0 \tag{3.15}$$

which defines the characteristic equation for the propagation of free natural waves on a dry multilayered plate.

By setting $\rho_b = 0$ (i.e., $Q_b = 0$) Eq. (3.14) reduces to

$$M_{21} + Q_u M_{11} = 0 \tag{3.16}$$

which defines the characteristic equation for free waves on the plate with one side of it kept free.

ACKNOWLEDGEMENT

The collaborative experimental effort by Dr. Dale E. Chimenti of the Material Laboratory at AFWAL has been of major importance to our theoretical modeling. Our combined efforts have resulted in several archival publications and a large number of presentations. For this I am greatful. The author is also pleased to acknowledge the competent assistance of T. W. Taylor.

Appendix A

$$C_{11} = C'_{11}G^4 + C'_{22}S^4 + 2(C'_{12} + 2C'_{66})S^2G^2$$

$$C_{12} = (C'_{11} + C'_{22} - 4C'_{66})S^2G^2 + C'_{12}(S^4 + G^4)$$

$$C_{13} = C'_{13}G^2 + C'_{23}S^2$$

$$C_{16} = (C'_{11} - C'_{12} - 2C'_{66})SG^3 + (C'_{12} - C'_{22} + 2C'_{66})GS^3$$

$$C_{22} = C'_{11}S^4 + 2(C'_{12} + 2C'_{66})S^2G^2 + C'_{22}G^4$$

$$C_{23} = C'_{23}G^2 + C_{13}S^2$$

$$C_{26} = (C'_{11} - C'_{12} - 2C'_{66})GS^3 + (C'_{12} - C'_{22} + 2C'_{66})SG^3$$

$$C_{33} = C'_{33}$$

$$C_{36} = (C'_{23} - C'_{13})SG$$

$$C_{45} = (C'_{44} - C'_{55})SG$$

$$C_{44} = C'_{44}G^2 + C'_{55}S^2$$

$$C_{55} = C'_{55}G^2 + C'_{44}S^2$$

$$C_{66} = (C'_{11} + C'_{22} - 2C'_{12} - 2C'_{66})S^2G^2 + C_{66}(S^4 + G^4)$$

Where $G = \cos \phi$ and $S = \sin \phi$.

Appendix B

The coefficients of Eq. (1.10) are given by

$$A_1 = (P_1F_{11} + P_2C_{55} - P_4F_{12} - P_5C_{45} + P_7F_{13})/\Delta$$

$$A_2 = (P_2F_{11} + P_3C_{55} - P_5F_{12} - P_6C_{45} + P_8F_{13})/\Delta$$

$$A_3 = (P_3F_{11} - P_6F_{12})/\Delta$$

$$\Delta = P_1C_{55} - P_4C_{45}$$

$$P_1 = C_{44}C_{55} \; ; \; P_3 = F_{22}F_{33}$$

$$P_2 = F_{23}C_{33} + F_{33}C_{44} - F_{23}$$

$$P_4 = C_{33}C_{45} \; , \; P_6 = F_{12}F_{32}$$

$$P_5 = C_{33}F_{12} + F_{33}C_{45} - F_{13}F_{23}$$

$$P_6 = F_{23}C_{45} - F_{13}C_{44} \; ; \; P_7 = F_{12}F_{23} - F_{13}F_{22}$$

$$F_{11} = C_{11} - \rho c^2$$

$$F_{12} = C_{16}$$

$$F_{13} = C_{13} + C_{55}$$

$$F_{22} = C_{66} - \rho c^2$$

$$F_{23} = C_{36} + C_{45}$$

$$F_{33} = C_{55} - \rho c^2$$

REFERENCES

1. M. J. P. Musgrave, Crystal Acoustics (Holden Day, San Francisco, 1970).
2. J. L. Synge, J. Math. Pys. 25, 323-334 (1957).
3. F. I. Fedorov, Theory of Elastic Waves in Crystals (Plenum, New York, 1968).
4. L.G. Merkulov, Appl. Mater. Res. 2, 231-240 (1963).
5. L.G. Merkulov and L.A. Yakovlev, Sov. Phys. Acoust. 8, 72-77 (1962).
6. L.G. Merkulov and L.A. Yakovlev, Sov. Phys. Acoust. 8, 152-155 (1962)
7. M.J.P. Musgrave, Geophys. J. 3, 406-418 (1960)
8. E. Gates, Appl. Phys. Lett. 7, 187-189 (1965).
9. N. Joel, Proc. Phys.Soc, Sect. A 78, 38 (1961).
10. E.G. Henneke, II,J. Acoust. Soc. Am. 51, 210 (1972).
11. T.C. Lim and M.J.P. Musgrave, Nature 225, 372 (1970).
12. W.W. Johnson,Bull. Seismol. Soc. Am. 60, 11005 (1970).
13. P.Chadwick and P.K. Currie, Q.J. Mech. Appl. Math XXVII, 497 (1974).
14. S.I. Rokhlin, T.K. Bolland and Laszlo Adler, J. Acoust. Soc. Am. 79(4), 906-918 (1986)
15. R. Stonley, Proc. Lond. Math. Soc. 232, 447 (1955).
16. V.T. Buchwald, Q.J. Mech. Appl. Math. 14, 461 (1961).
17. V.T. Buchwald and A. Davis, Nature (Lond.) 191, 899 (1961).
18. V.T. Buchwald and A. Davis, Q. J. Mech.Appl. Math 16 283 (1963).
19. D.C. Gazis, R. Herman, and R.F. Wallis, Phys. Rev. 119, 533 (1960).
20. F.R. Rollins, T.C. Lim, and G.W. Farnell, Appl. Phys. Lett. 12, 236 (1968).
21. T.C. Lim and G.W. Farnell, J. Acoust. Soc. Am. 45, 845 (1969).
22. See, for example, the series Physical Acoustics, ed. by W.P. Mason and,R. N. Thurston (Academic Press, New York).
23. S.A. Markus, M.D. Kaplan, and S.V. Veremeenko, Defektoskopiya 21, 3

(1985) [Sov.J. Nondestr. Test. 21 739 (1985)].

24. Zh. G. Nikiforenko, V. T. Bobrov, and I. I. Averbukh, Defektoskopiya 8, 56 (1972) [Soc. J. Nondestr. Test. 8, 543 (1972)].

25. I. Abubakar, Quart. J .Mech. and Appl. Math. (Part I), 15, 29 (1962)

26. Yu. A. Kosevich and E. S. Syrkin, Sov. Phys. Acoust. 31, 365 (1985).

27. E.R. Baylis and W. A. Green, Journal of Sound and Vibration 110(1),1-26 (1986).

28. L. G. Merkulov and D. A. Tursonov, Sov. Phys. Acoust. 15, 115 (1969).

29. L. P. Solie and B. A. Auld, J. Acoust. Soc. Am. 54(1), 50-65, (1973).

30. A. T. Jones, J. Comp. Mater. 4, 476 (1970).

31. S. V. Kulkarni and N. J. Pagano, J. Sound Vibr. 23, 127 (1972).

32. S.K. Datta, A.H. Shah, R.L. Bratton and T. Chakraborty, J. Acoust. Soc. Am. 83, 2020 (1988).

33. D. E. Chimenti and A. H. Nayfeh, J. Appl. Phys. 58 4531 (1985).

34. A. H. Nayfeh and D. E. Chimenti, J. Acoust. Soc. Am. 83, 1736 (1988).

35. L. M. Brekhovskikh, Waves in Layered Media, (Academic Press, New York, 1960).

36. I. A. Viktorov, Rayleigh and Lamb Waves, (Plenum,New York, 1967).

37. W. T. Thomson, J. Appl. Phys. 21, 89 (1950);ibid. 21, 1215 (1950).

38. A. E. H. Love, A Treatise on the Mathematical Theory of Elasticity, 4th ed. Dover, New York, N.Y., 1927.

39. H. Lamb, Proc. Roy. Soc. (London), Ser. A, 93, 114 (1917).

40. C'_{11}, C'_{22}, C'_{33}, C'_{13}, C'_{23}, C'_{44}, C'_{55} are given by 155.6, 11.5, 15.95, 3.72, 4.33, 5.81, 6.5 GPa, respectively, ρ = 1.6 g/cm^3, c_f = 1.48 km/sec and ρ_f = 1 g/cm^3.

41. D.E. Chimenti and A.H. Nayfeh, Appl. Phys. Letters 49, 492 (1986).

42. L. Cremer, Akust. Z. 7, 81 (1942).

43. M. Knight, J. Composite Mat. 16, 153 (1982).

44. W. Prosser, M.S. Thesis, Johns Hopkins Univ., 1987 (unpublished).

45. A. H. Nayfeh and D. E. Chimenti, accepted and to appear in Journal of Applied Mechanics.

46. D. E. Chimenti and A. H. Nayfeh, J. Acoust. Soc. Am. 85, (1989).

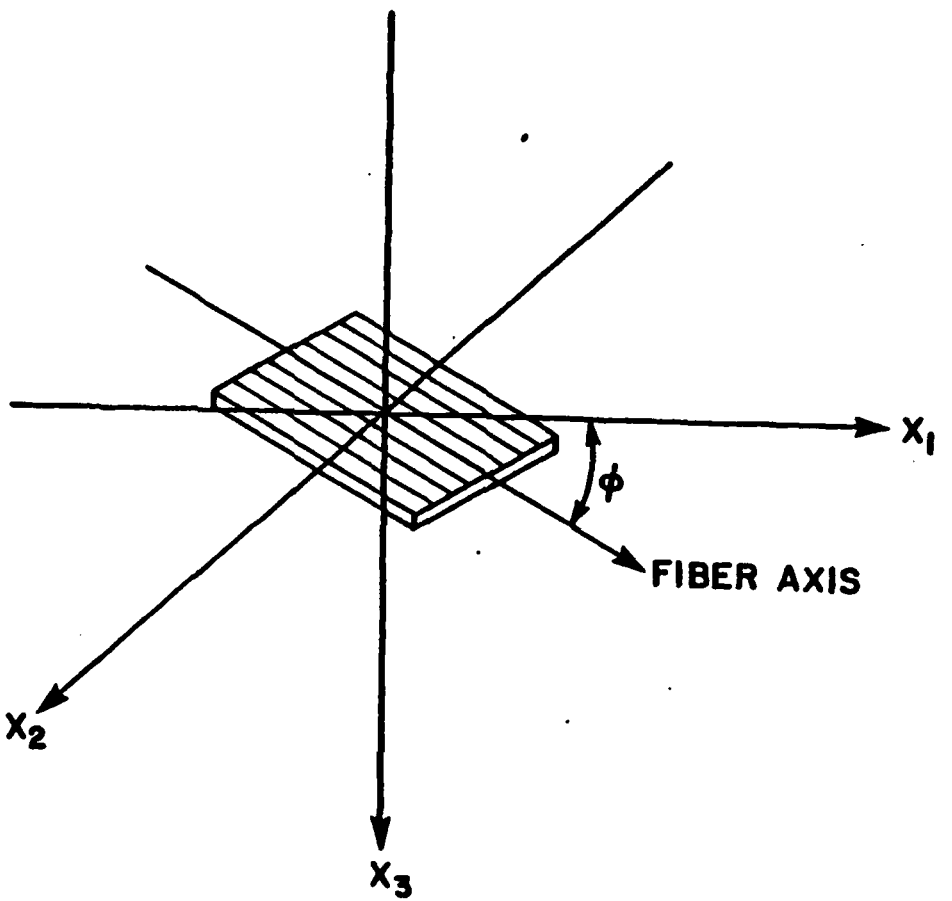

Figure 1.1. Coordinate system for leaky plate wave problem. Incident beam strikes plate at angle θ, and ϕ is angle between fiber axis and plane of incidence.

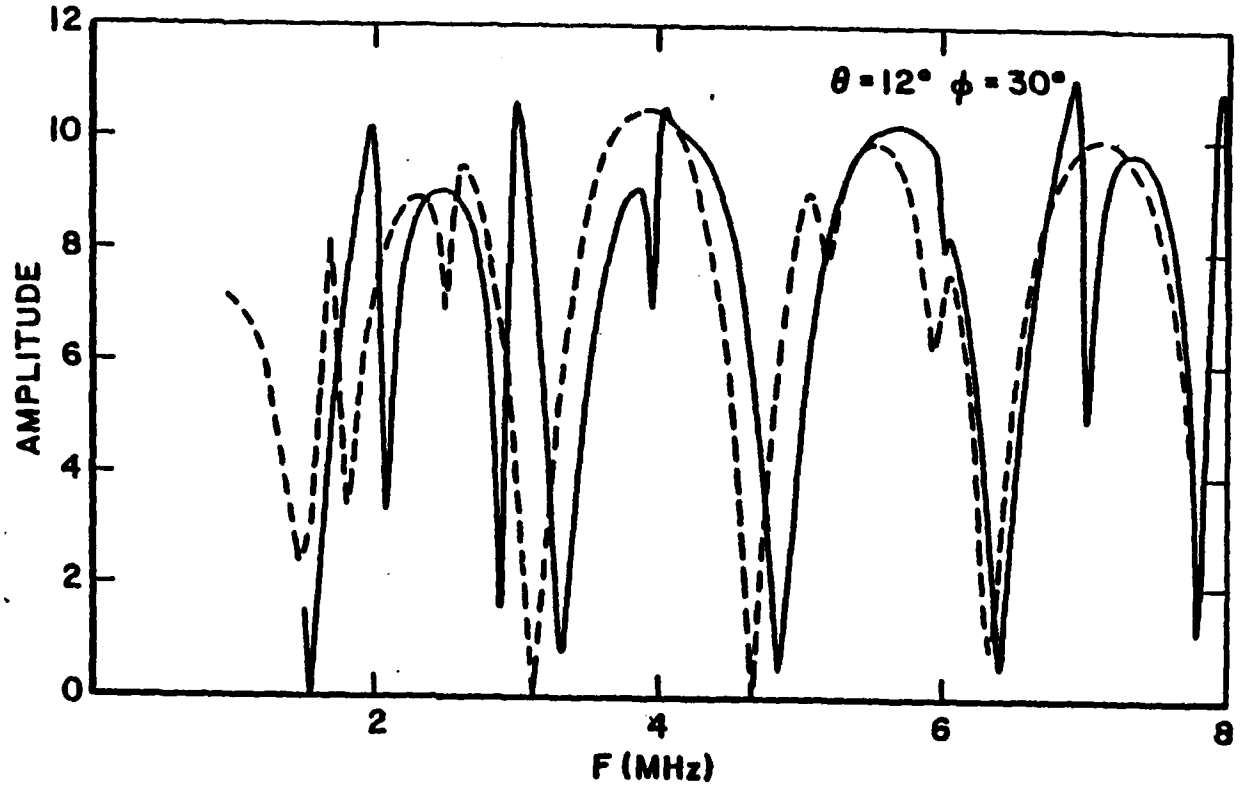

Figure 1.2(a). Reflection (plate-wave) spectrum for θ = 12° and ϕ = 30°. Theory is solid curve and experiment is dashed curve. Data has been deconvolved to remove transducer response.

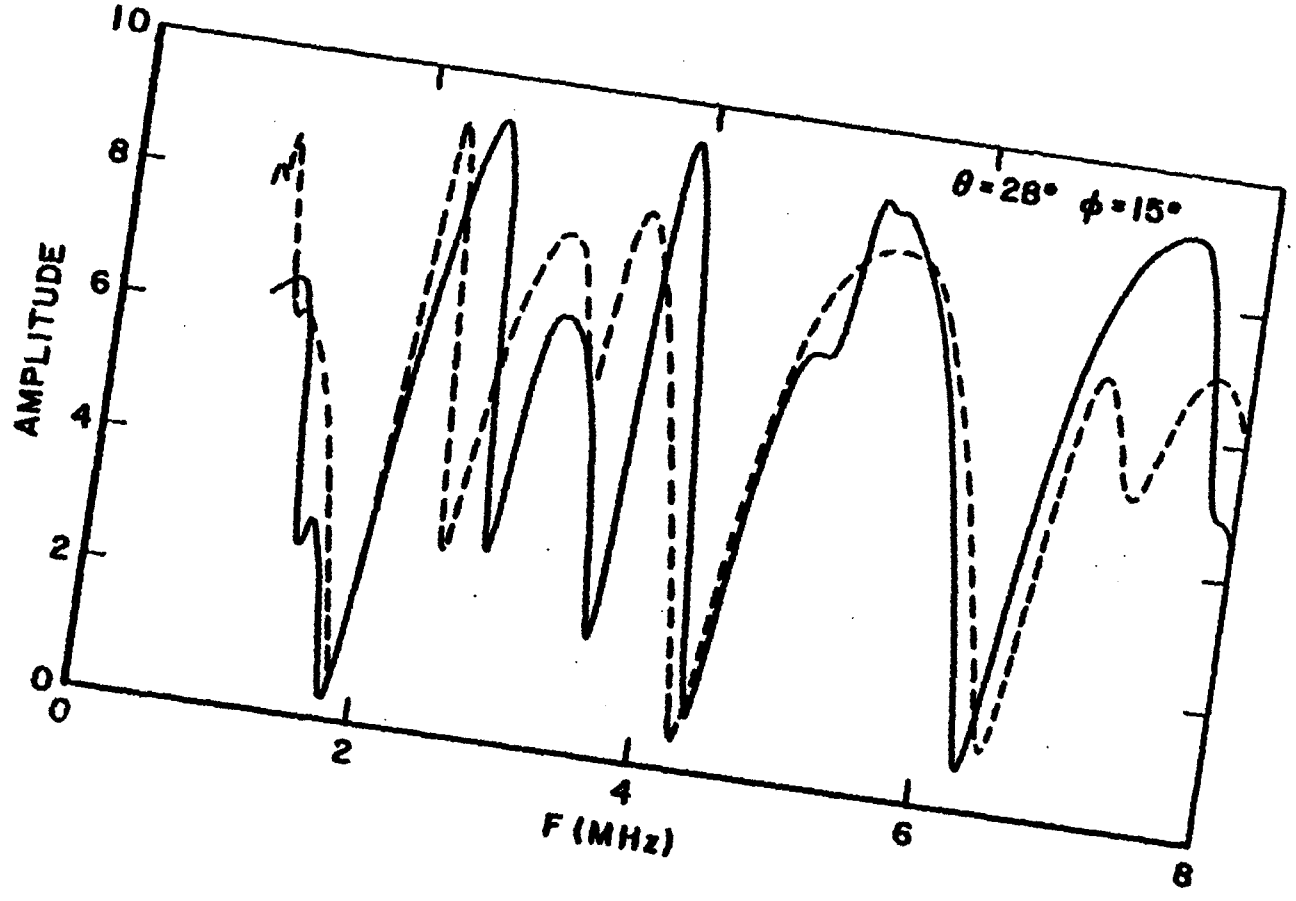

Figure 1.2(b). Reflection spectrum for $\theta = 28°$ and $\phi = 15°$.

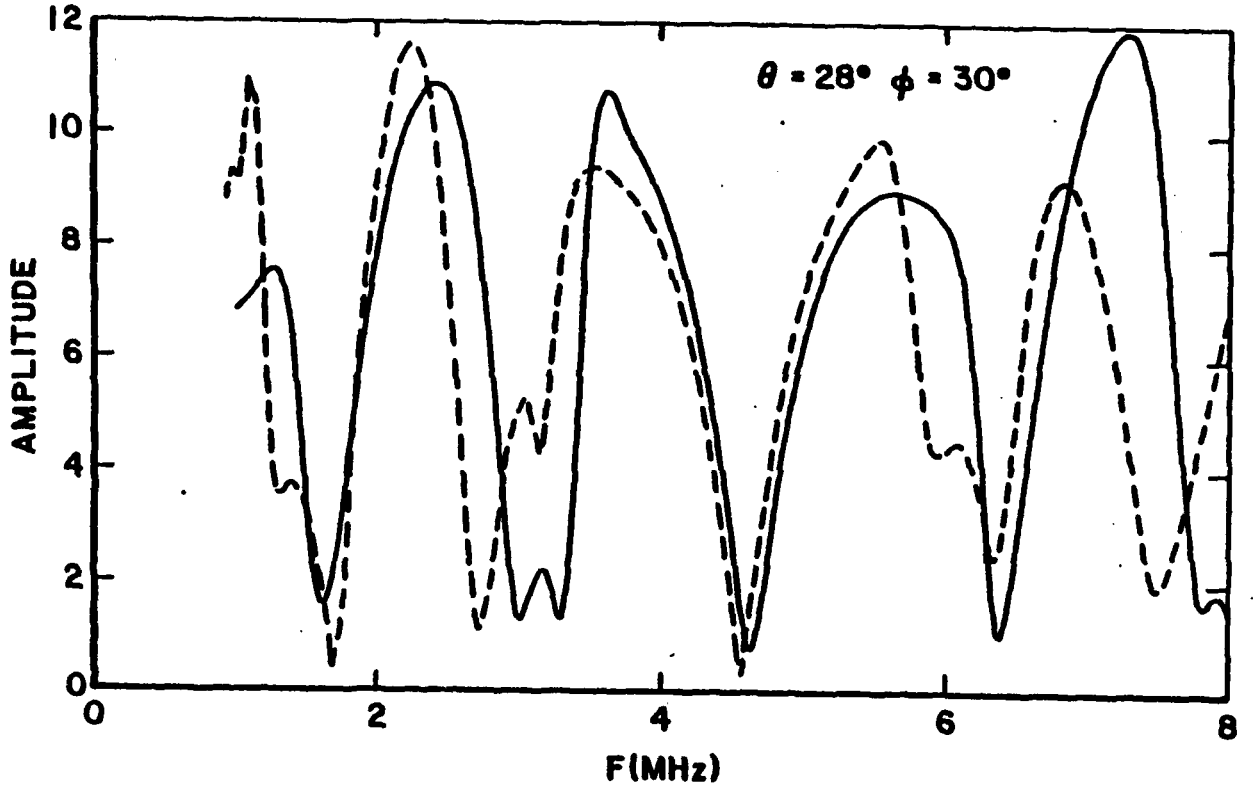

Figure 1.2(c). Reflection spectrum for θ = 28° and ϕ = 30°.

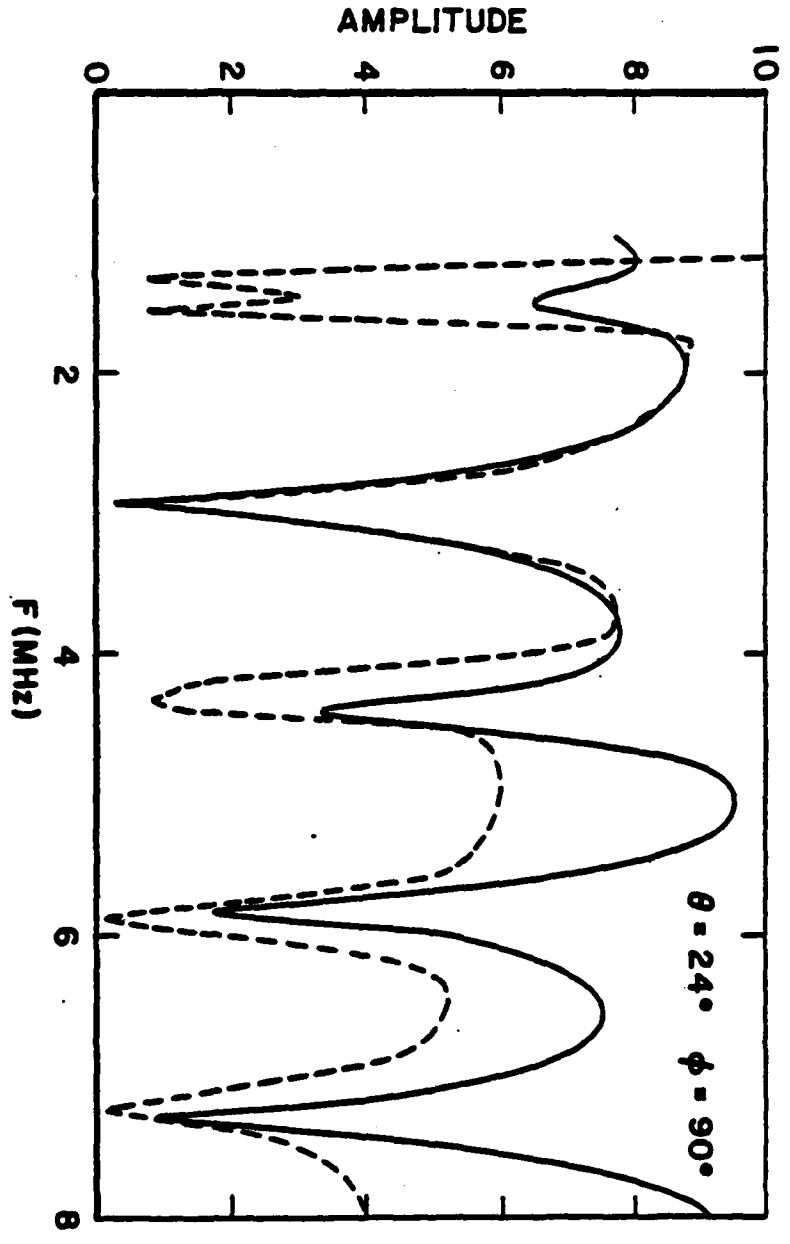

Figure 1.2(d). Reflection spectrum for $\theta = 24°$ and $\phi = 90°$.

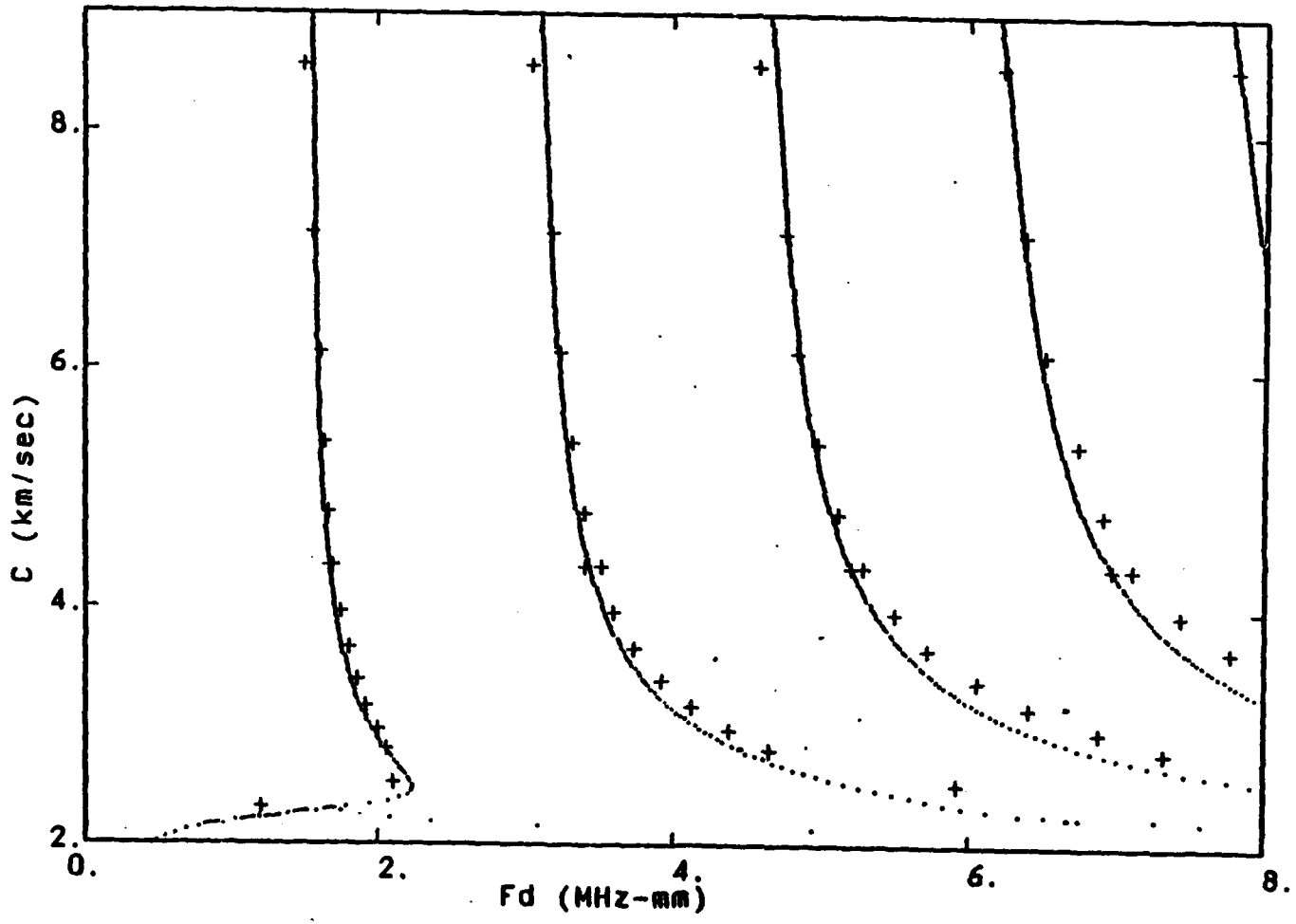

Figure 1.3(a) Reflection results expressed as phase velocity dispersion curves for $\phi = 0°$. Data are plotted as discrete crosses; theory curves are small filled circles. In some regions of the theory curves dashed lines have been added as a guide to the eye.

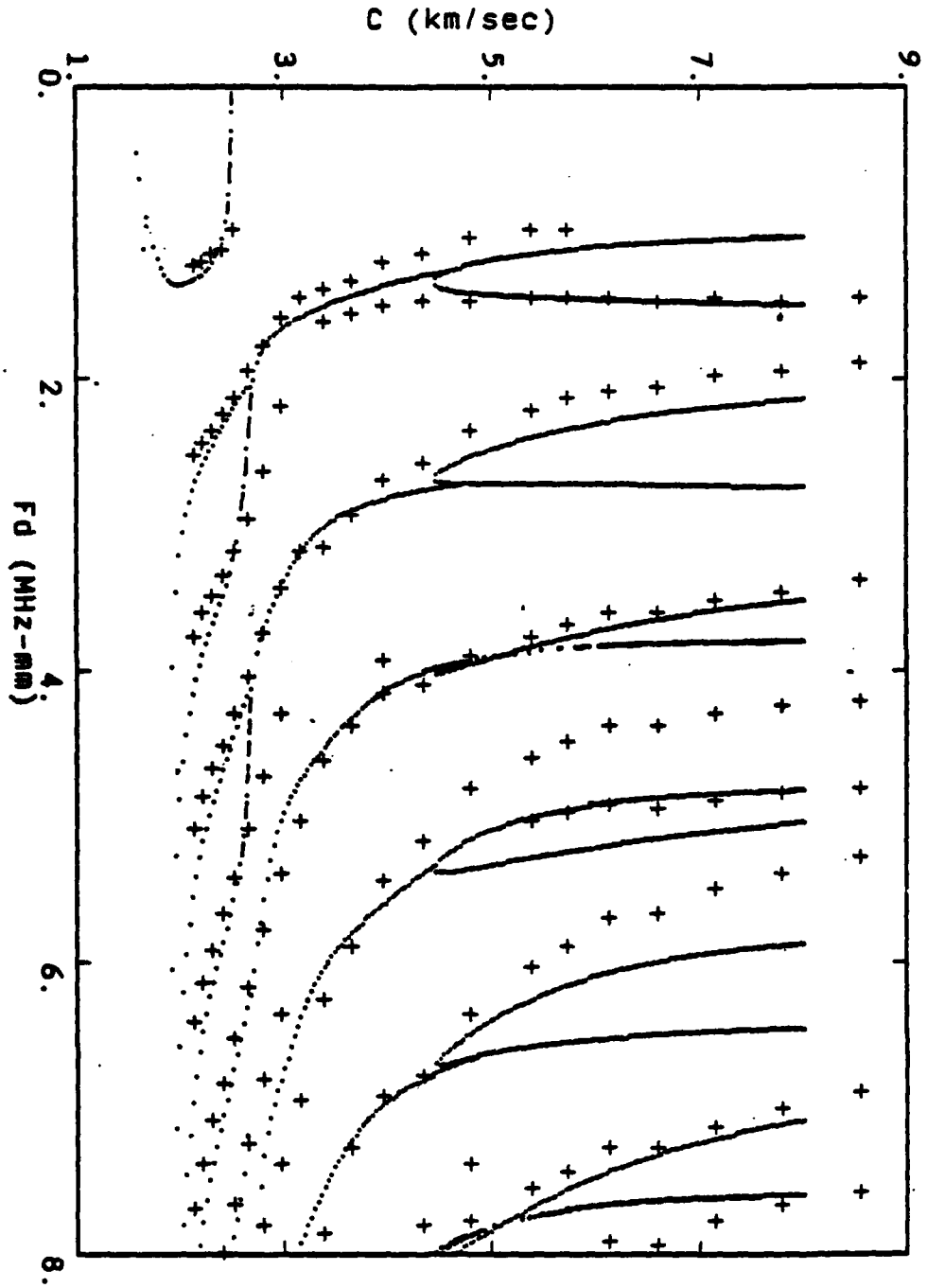

Figure 1.3(b) Dispersion plot for $\phi = 90°$. Data are crosses; theory curves are small filled circles.

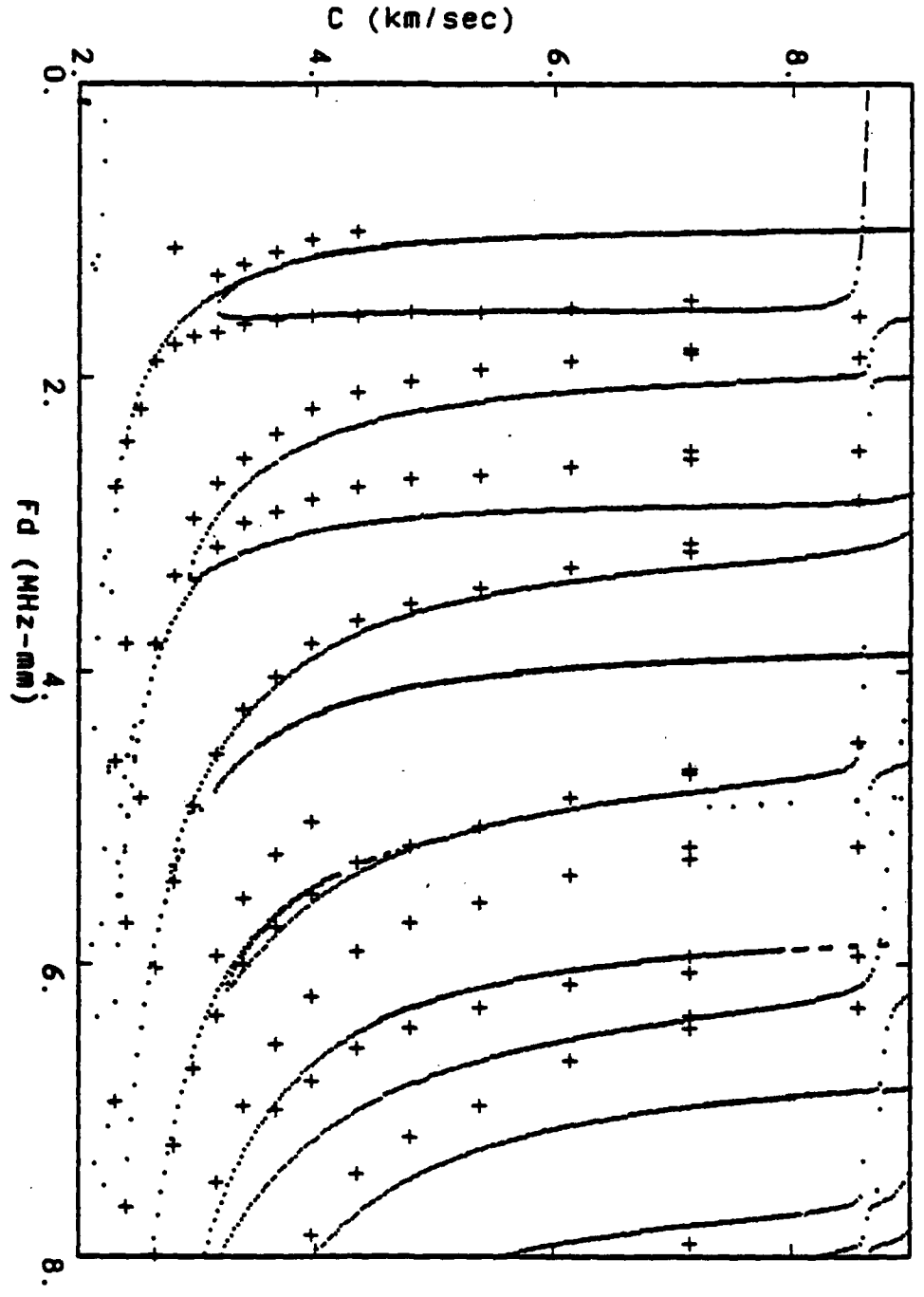

Figure 1.4(a). Dispersion plot for ϕ = 30°.

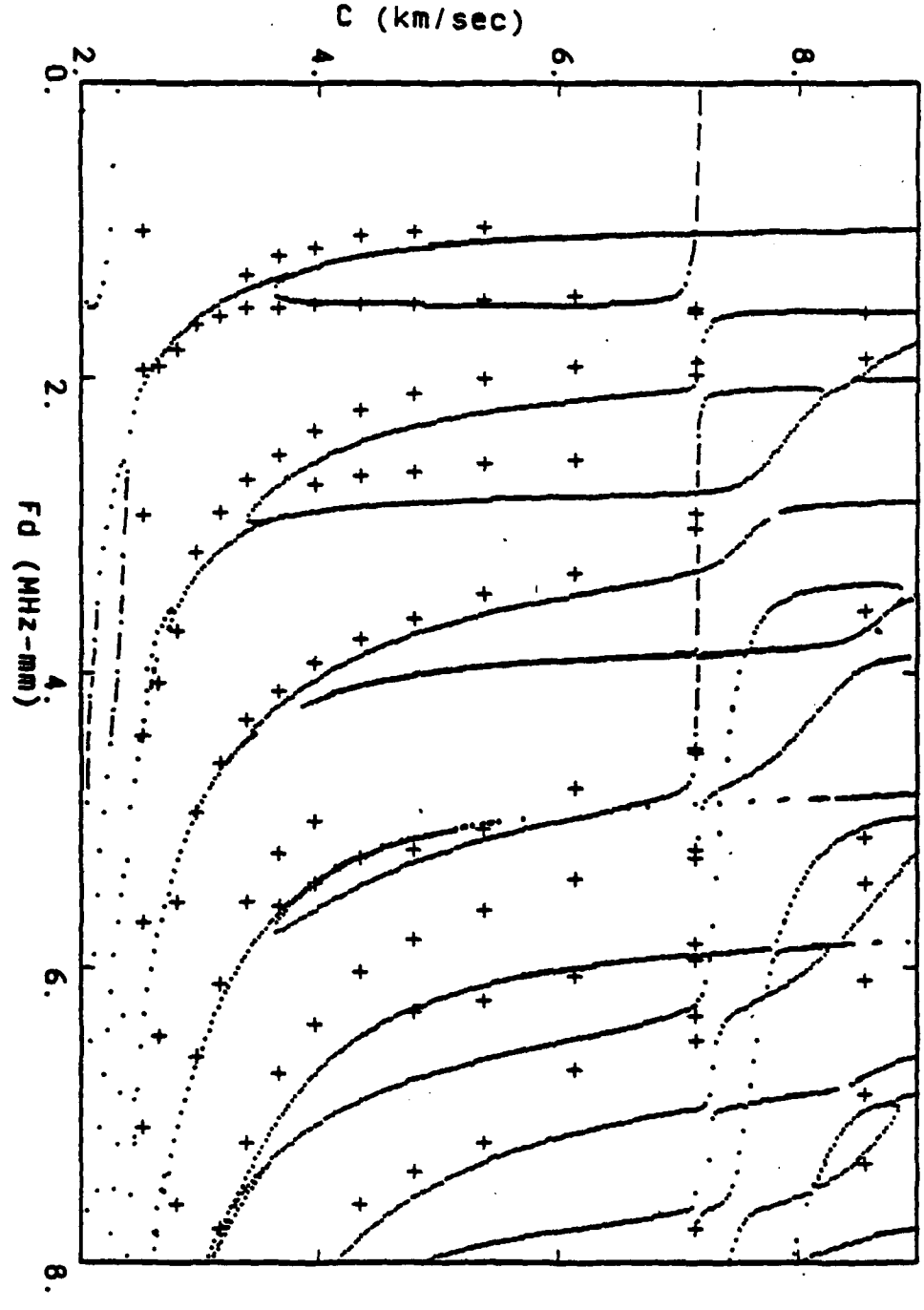

Figure 1.4(b) Dispersion plot for ϕ = 45°.

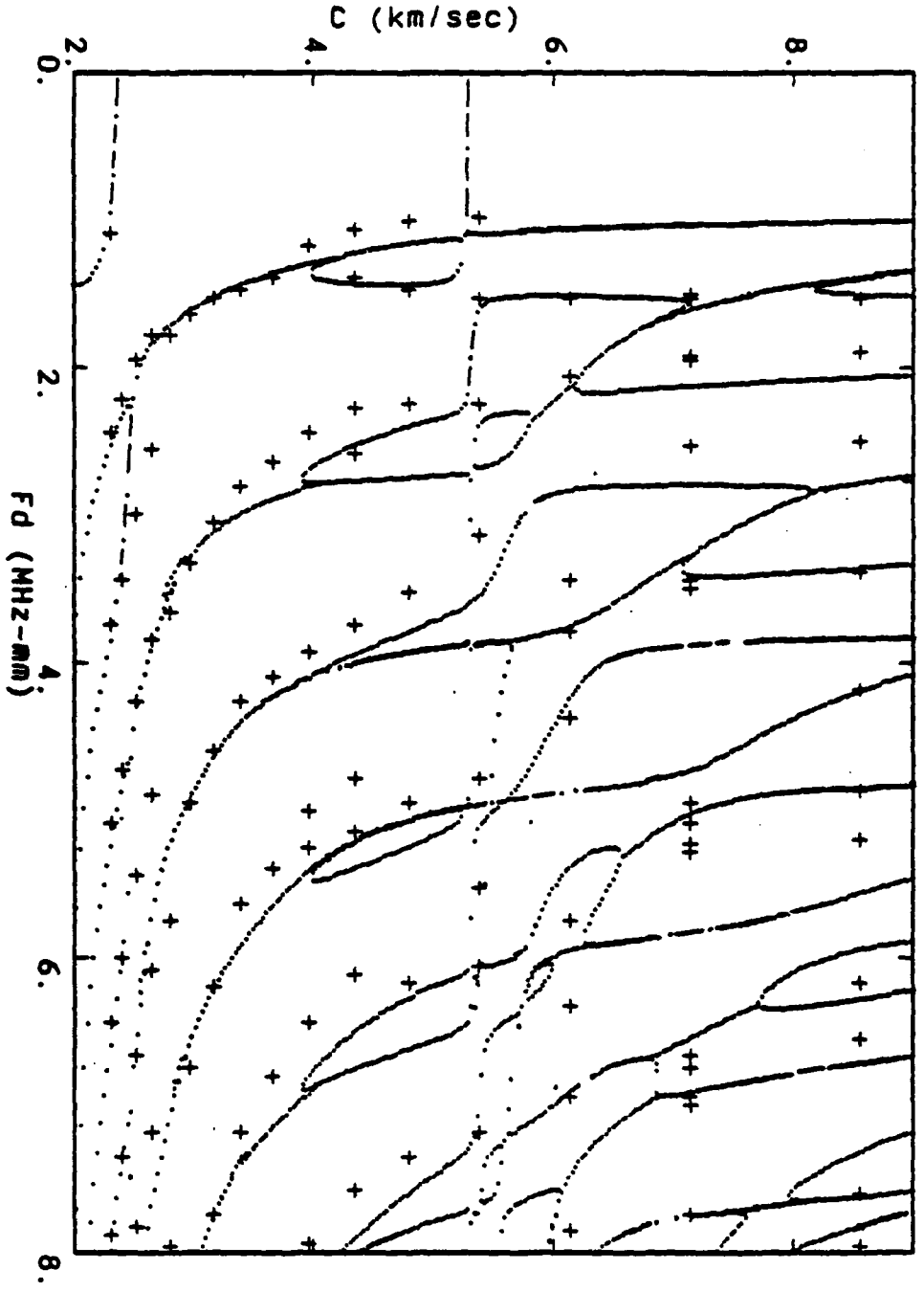

Figure 1.4(c) Dispersion plot for $\phi = 60°$.

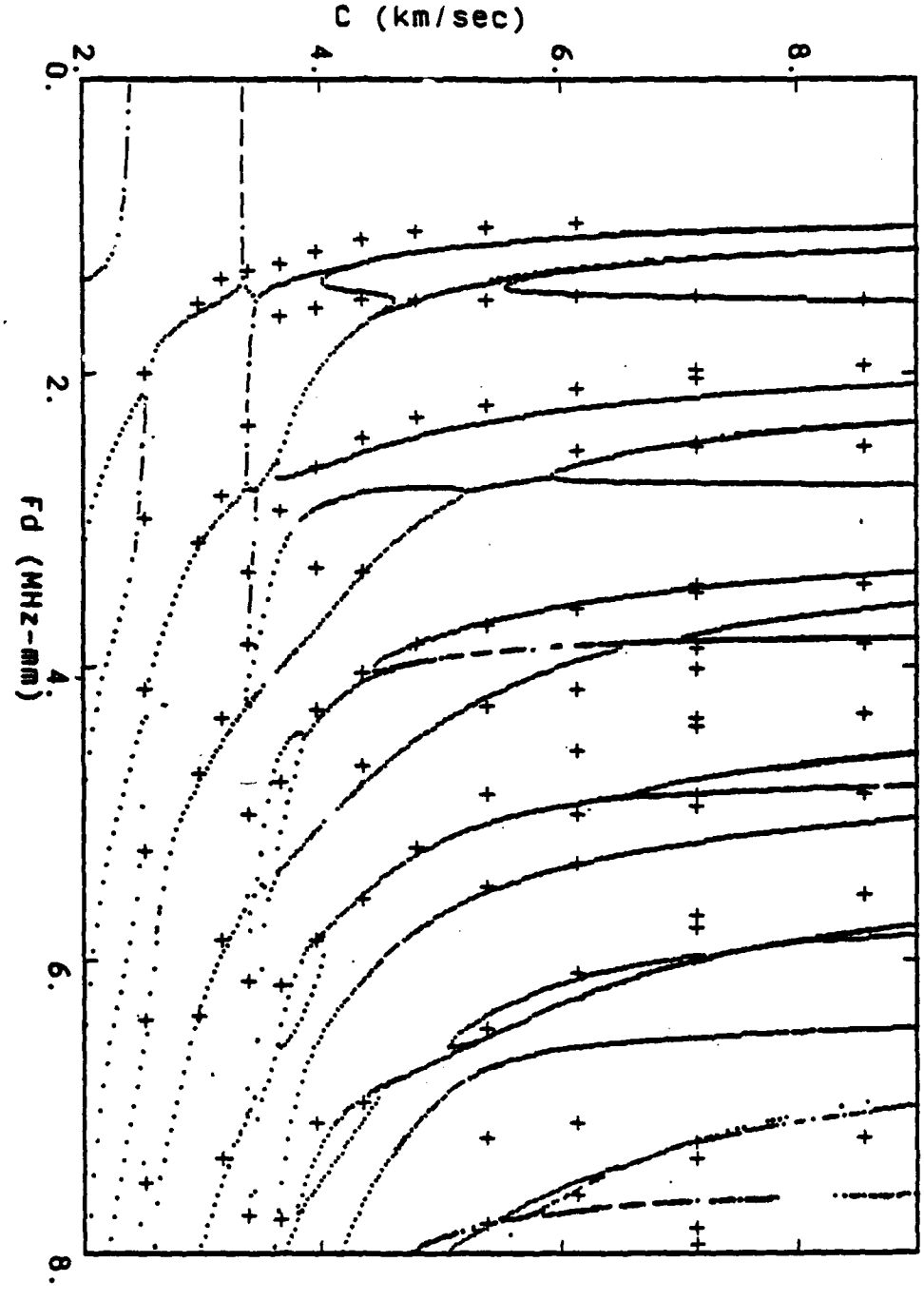

Figure 1.4(d). Dispersion plot for ϕ = 75°.

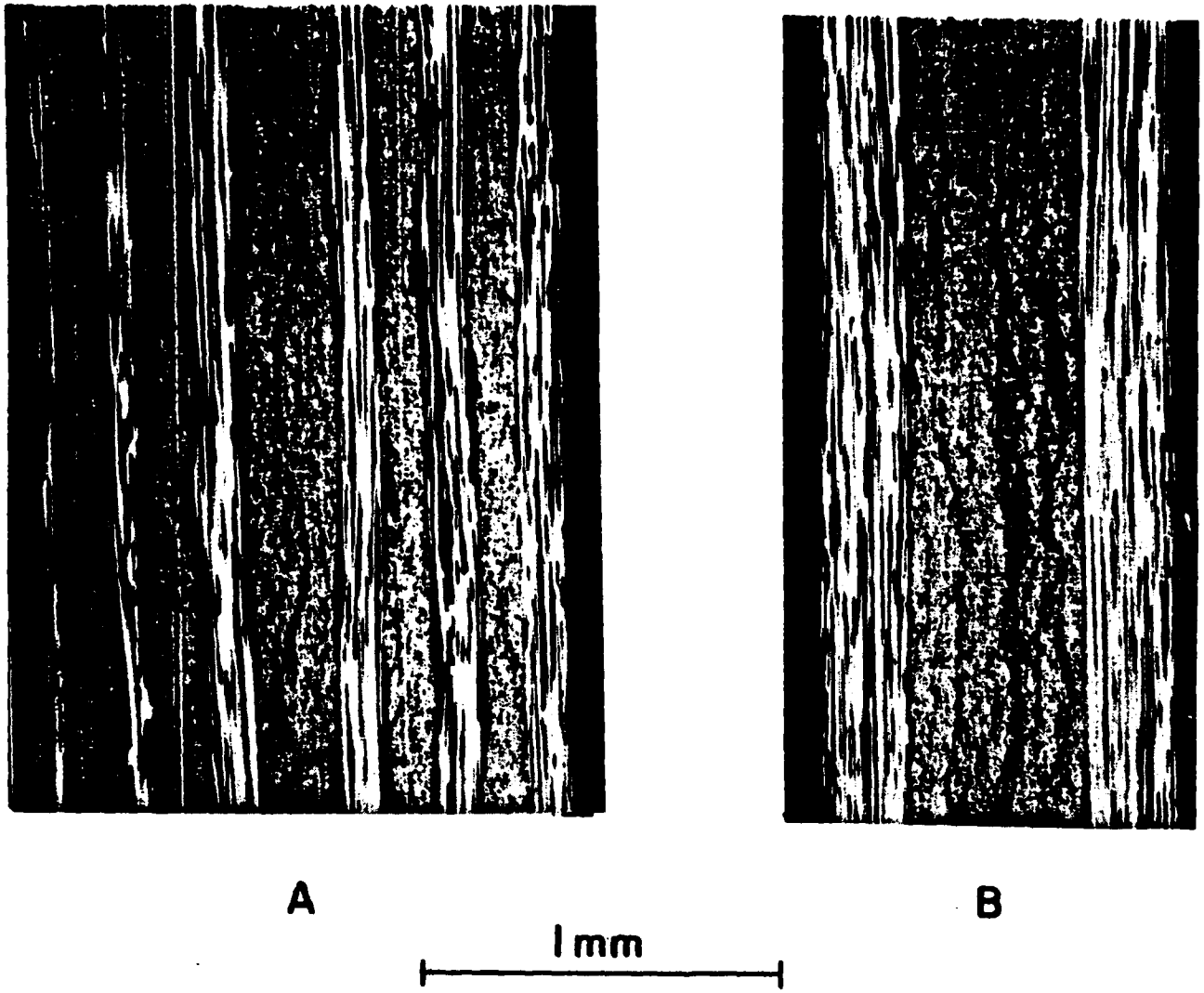

Fig. 2.1. Optical micrographs of composite specimens on which experiments have been performed. Sample A is the $[0,90]_{3s}$ layup, while the $[0_2,90_2]_s$ sample is shown in frame B. The degree of uniformity of fiber distribution in these samples is typical of this material.

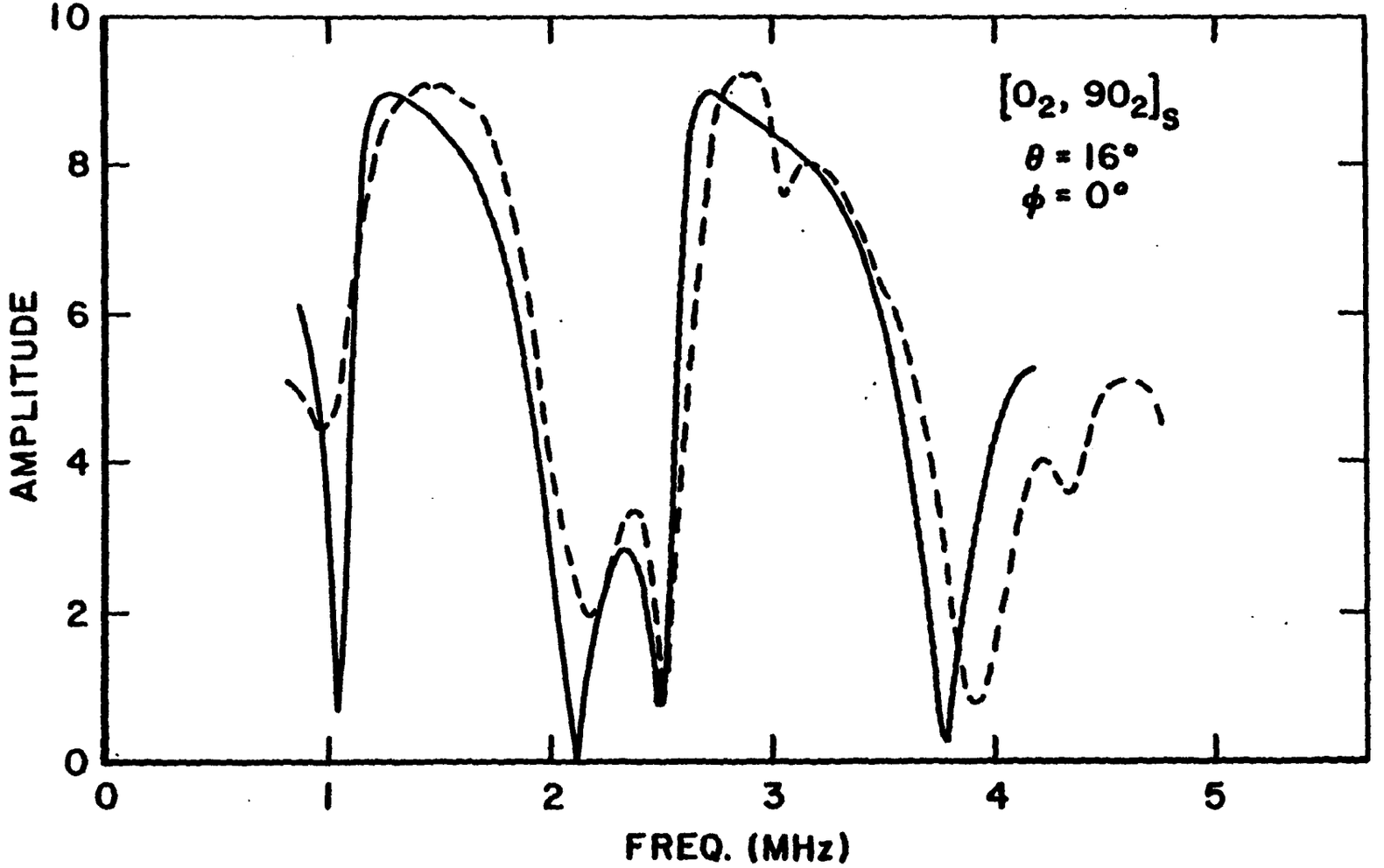

Fig. 2.2. Experimental (dashed) and theoretical (solid) reflection spectrum for the $[0_2, 90_2]_s$ laminate with an incident angle of 16° and with the fiber direction of the uppermost ply in the incident plane.

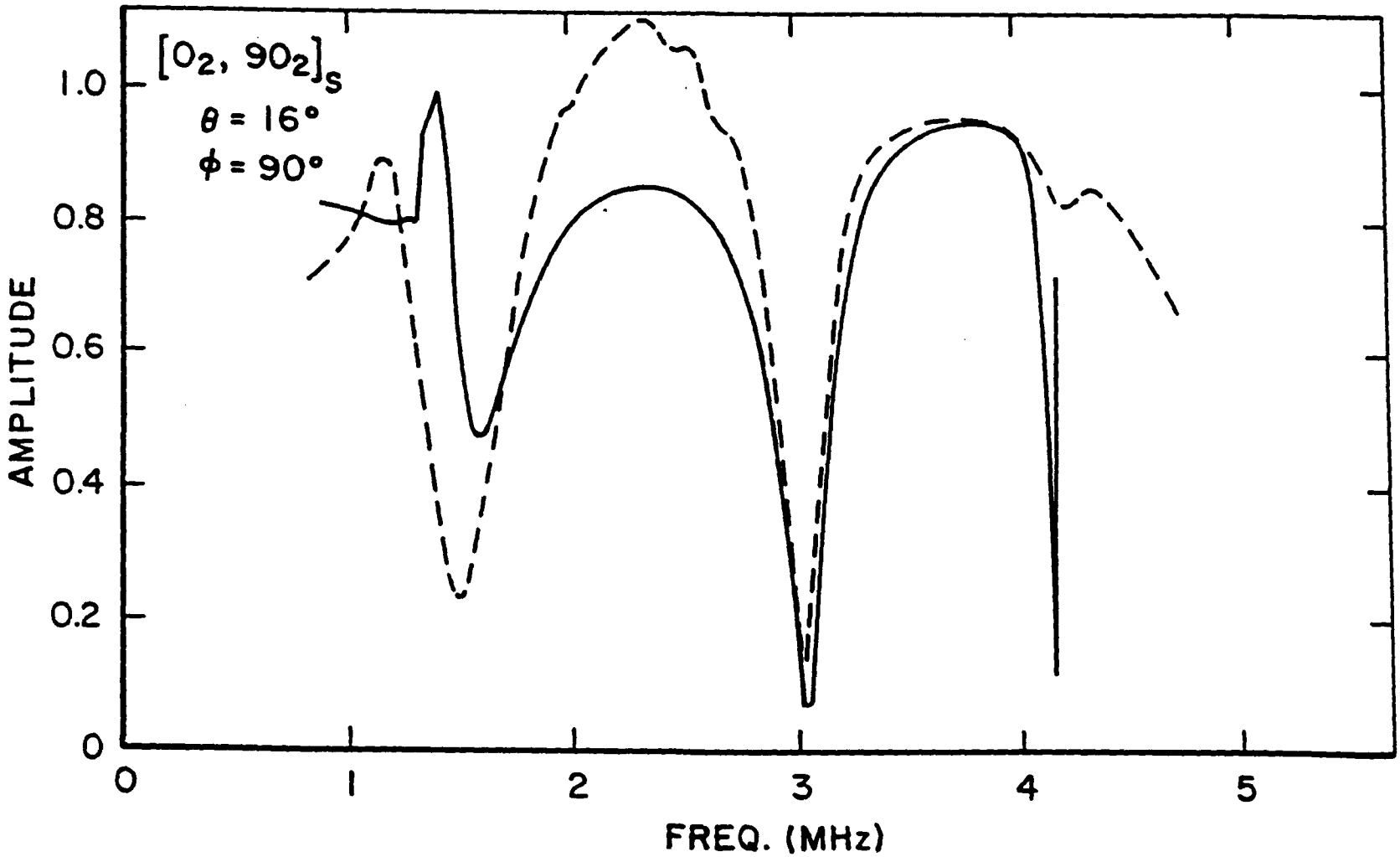

Fig. 2.3. Reflection spectrum for same conditions as in Fig. 2.2 but with the fiber direction in the uppermost ply perpendicular to the incident plane. This variation corresponds to the reversal of the layer ordering. Yet, the reflection behavior is completely different. Measurement is dashed curve; theory is solid curve.

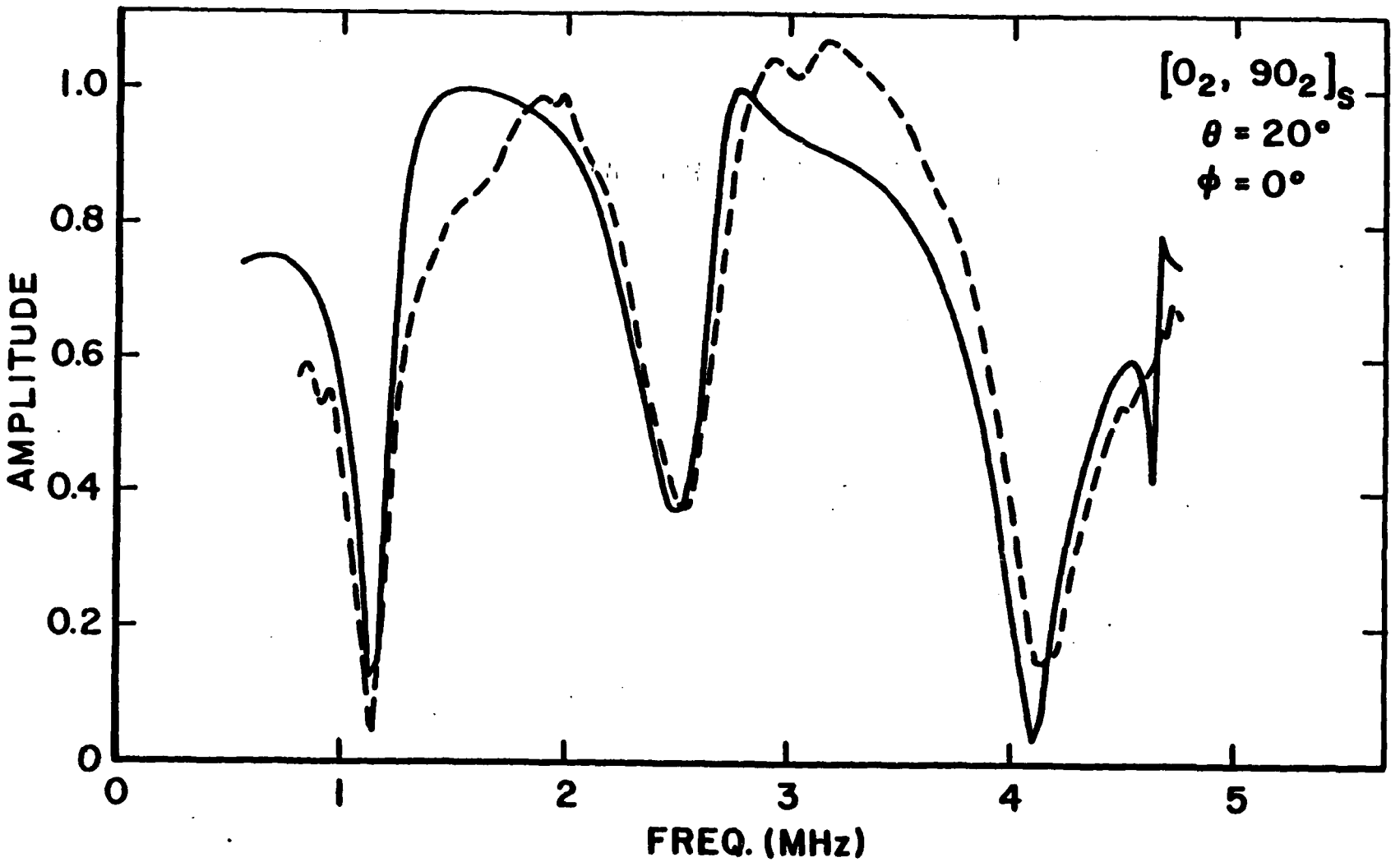

Fig. 2.4. Reflection spectrum for same sample as in Figs. 2.2 and 2.3 where incident angle is 20°. Fiber direction in uppermost ply lies in the incident plane.

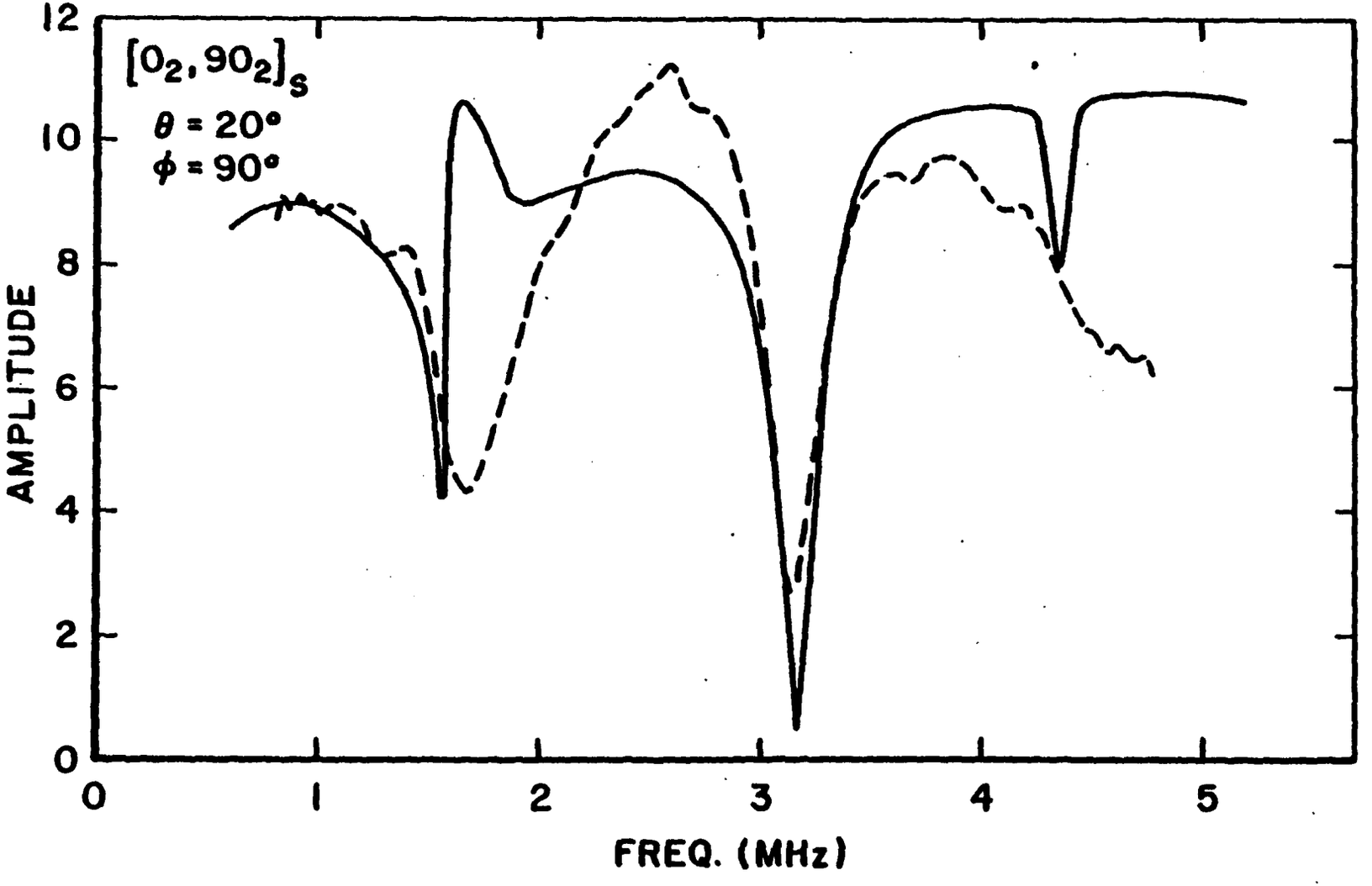

Fig. 2.5. Conditions of Fig.2.4with uppermost ply fiber direction normal to incident plane. Experimental curve is dashed; theory curve is solid.

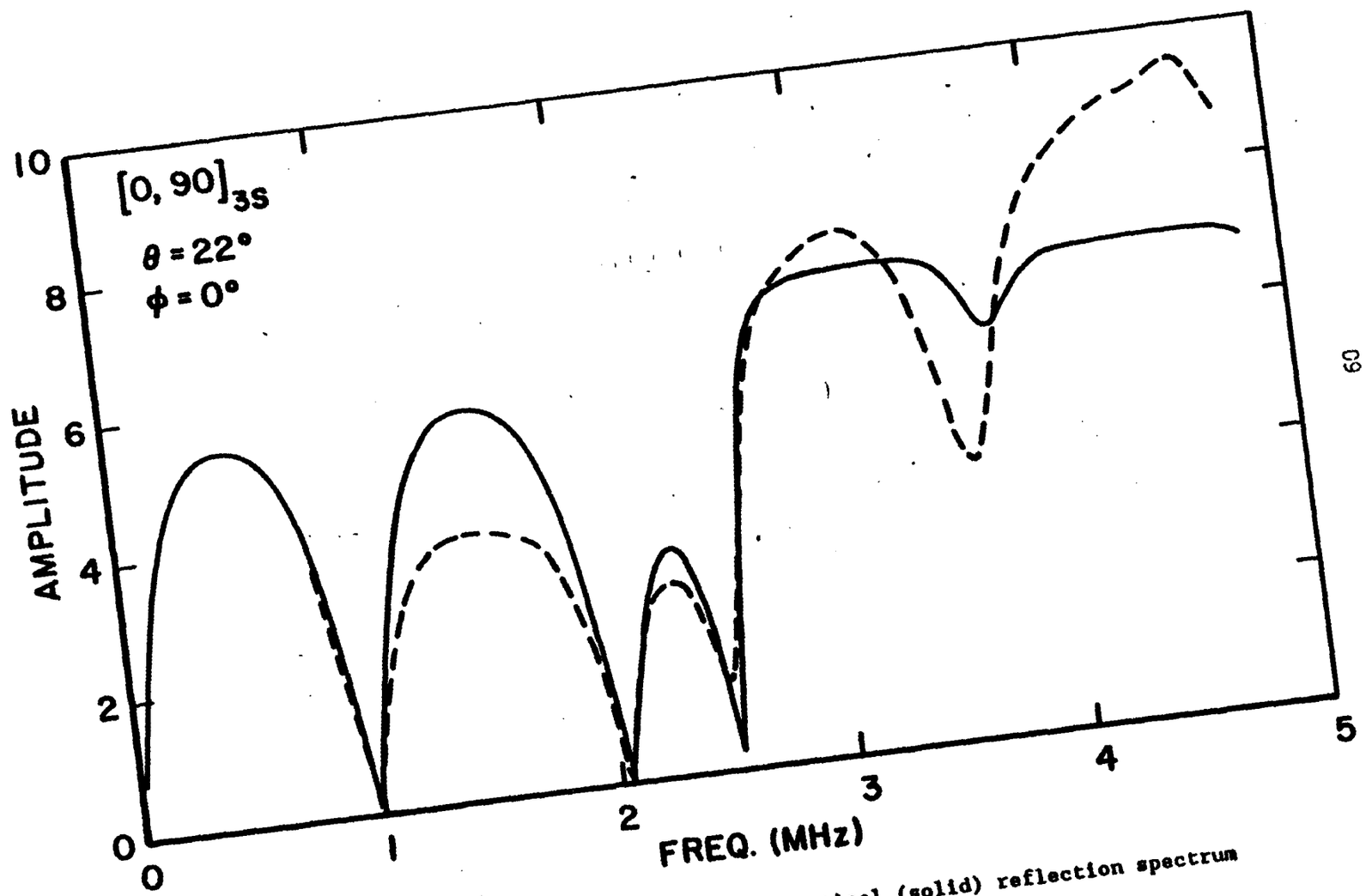

Fig. 2.6. Experimental (dashed) and theoretical (solid) reflection spectrum for the $[0, 90]_{3s}$ laminate with an incident angle of 22° and with the fiber direction in the uppermost ply in the incident plane.

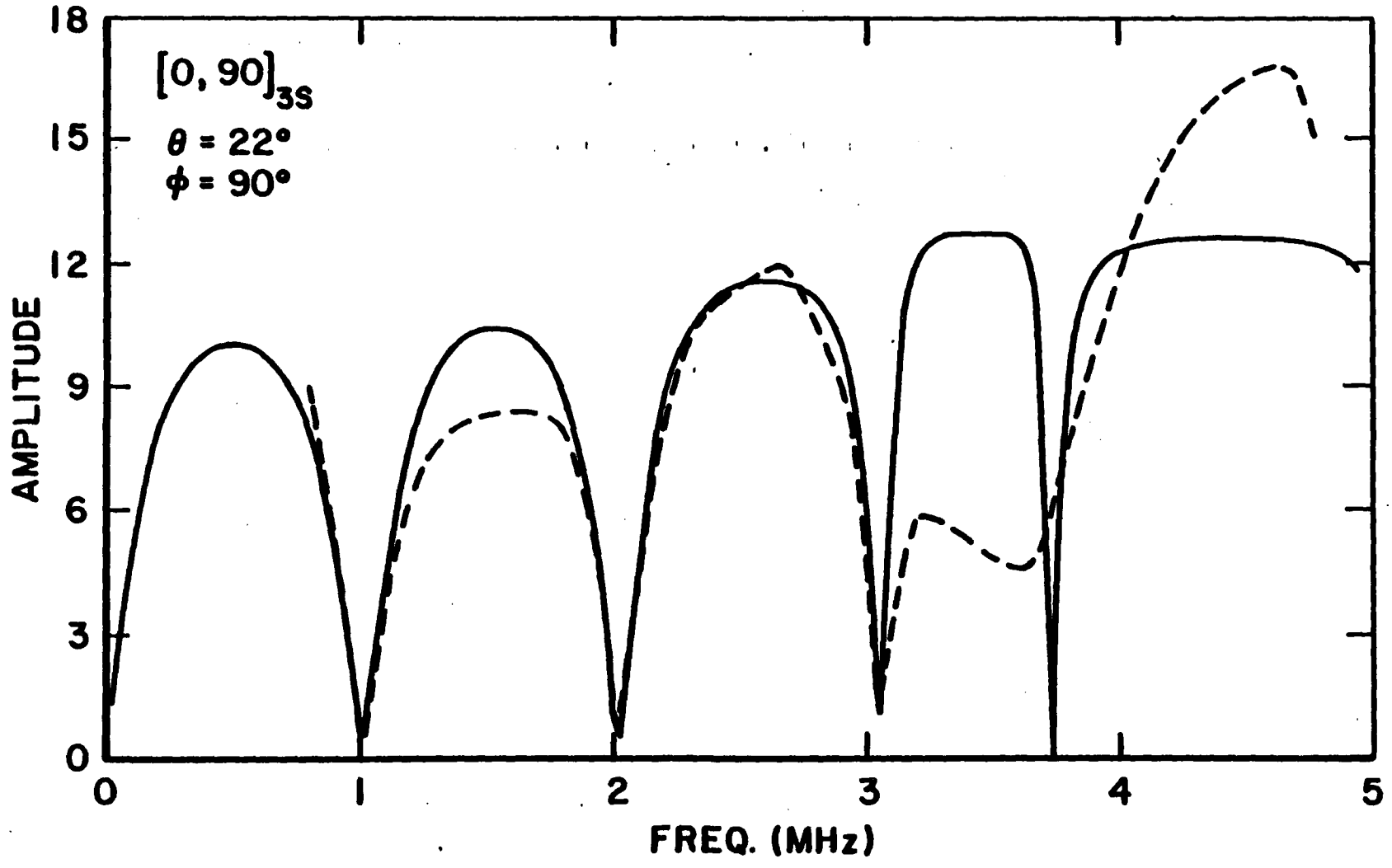

Fig. 2.7. Reflection spectrum as in Fig. 2.6 but with fiber direction in top ply normal to incident plane. At low frequencies little change from Fig. 2.6 is seen; above 2.5 MHz significant differences appear.

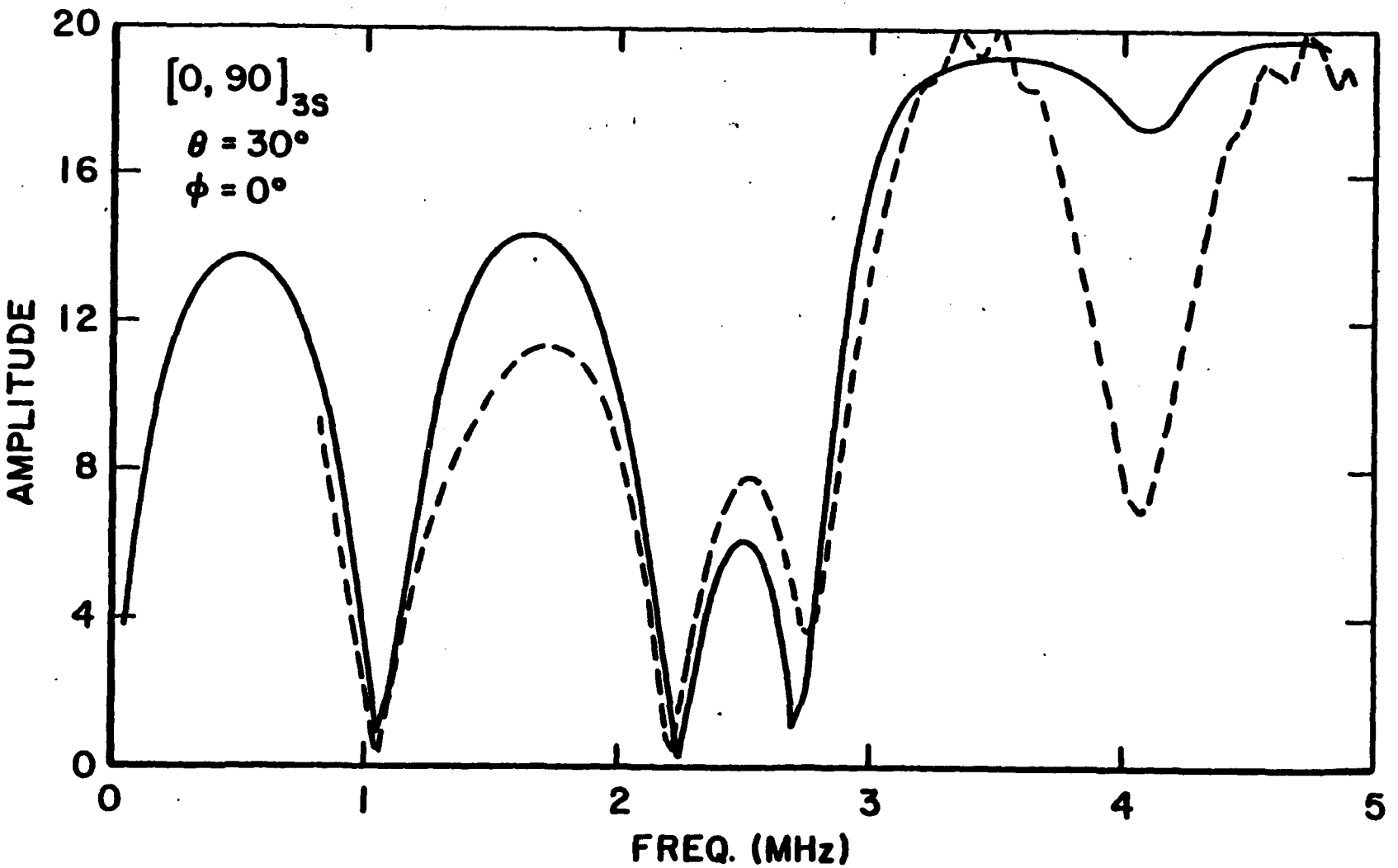

Fig. 2.8. As in Fig. 2.6 but at an incident angle of 30°. Small amplitude oscillations on peaks near 3.5 and 4.7 MHz are experimental artifacts. Theory curve is solid.

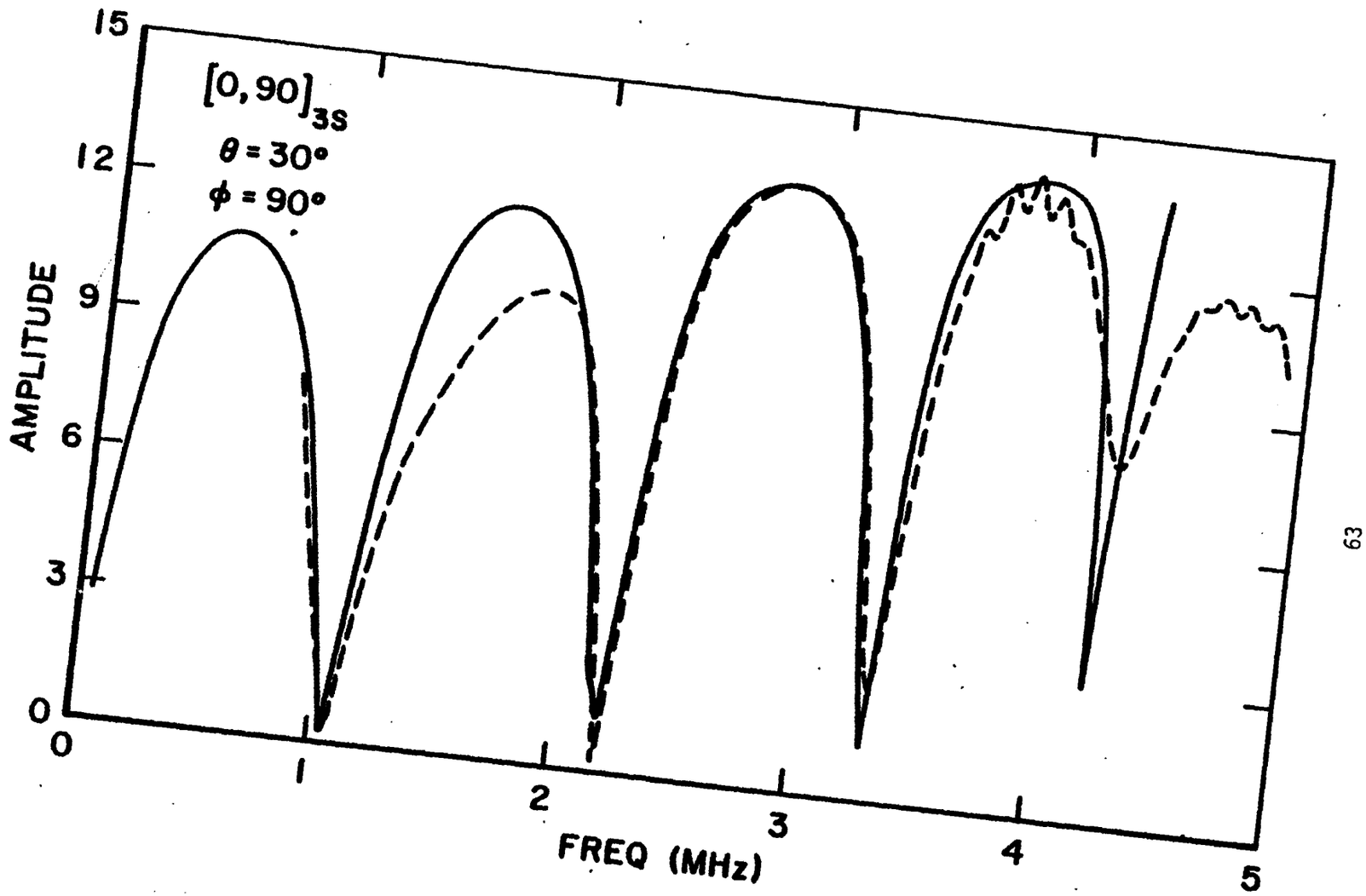

Fig. 2.9. As in Fig. 2.8 but with top ply fiber direction normal to incident plane.

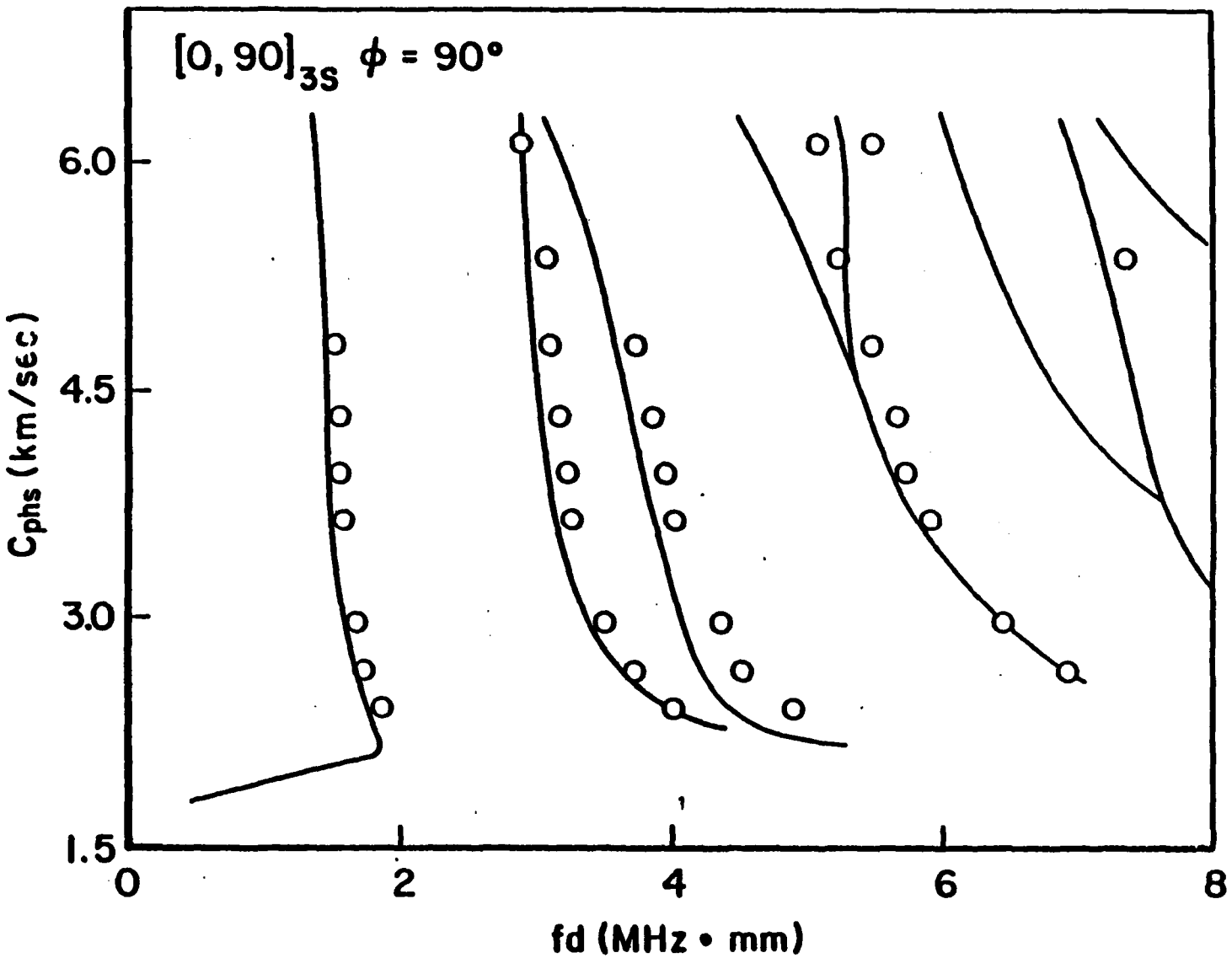

Fig. 2.10. Reflection-derived velocity dispersion curve for the $[0_2, 90_2]_s$ specimen with the fiber direction in the top ply normal to the incident plane. Measurements are plotted as open circles, while theory is solid curve.